AFGL-TR-88-0154

Alternatives to Mie Theory

David R. Longtin
Eric P. Shettle

OptiMetrics, Inc
50 Mall Road
Burlington, MA 01803

June 1988

Scientific Report No. 7

AIR FORCE GEOPHYSICS LABORATORY
AIR FORCE SYSTEMS COMMAND
UNITED STATES AIR FORCE
HANSCOM AIR FORCE BASE, MASSACHUSETTS 01731-5000

"This technical report has been reviewed and is approved for publication"

ERIC P. SHETTLE
Contract Manager

DONALD E. BEDO
Branch Chief

FOR THE COMMANDER

R. EARL GOOD
Division Director

This report has been reviewed by the ESD Public Affairs Office (PA) and is releasable to the National Technical Information Service (NTIS).

Qualified requestors may obtain additional copies from the Defense Technical Information center. All others should apply to the National Technical Information Service.

If your address has changed, or if you wish to be removed from the mailing list, or if the addressee is no longer employed by your organization, please notify AFGL/DAA, Hanscom AFB, MA 01731. This will assist us in maintaining a current mailing list.

Do not return copies of this report unless contractual obligations or notices on a specific document requires that it be returned.

UNCLASSIFIED
SECURITY CLASSIFICATION OF THIS PAGE

REPORT DOCUMENTATION PAGE

1a REPORT SECURITY CLASSIFICATION Unclassified	1b RESTRICTIVE MARKINGS
2a SECURITY CLASSIFICATION AUTHORITY	3 DISTRIBUTION / AVAILABILITY OF REPORT approved for public release; distribution unlimited
2b DECLASSIFICATION / DOWNGRADING SCHEDULE	
4 PERFORMING ORGANIZATION REPORT NUMBER(S) OMI-293	5 MONITORING ORGANIZATION REPORT NUMBER(S) AFGL-TR-88-0154
6a NAME OF PERFORMING ORGANIZATION OptiMetrics, Inc. — 6b OFFICE SYMBOL (If applicable)	7a NAME OF MONITORING ORGANIZATION Air Force Geophysics Laboratory
6c ADDRESS (City, State, and ZIP Code) 50 Mall Road, Suite 211 Burlington, MA 01803-4998	7b ADDRESS (City, State, and ZIP Code) Hanscom Air Force Base Massachusetts 01731
8a NAME OF FUNDING / SPONSORING ORGANIZATION Air Force Geophysics Lab. — 8b OFFICE SYMBOL (If applicable)	9 PROCUREMENT INSTRUMENT IDENTIFICATION NUMBER F19628-85-C-0178
8c ADDRESS (City, State, and ZIP Code) Hanscom AFB, MA 01731	10 SOURCE OF FUNDING NUMBERS PROGRAM ELEMENT NO: 62101F 62101F — PROJECT NO: 7670 7670 — TASK NO: 15 15 — WORK UNIT ACCESSION NO: 16* AI

11 TITLE (Include Security Classification)
Alternatives to Mie Theory

12 PERSONAL AUTHOR(S)
David R. Longtin and Eric P. Shettle**

13a TYPE OF REPORT	13b. TIME COVERED	14 DATE OF REPORT (Year, Month, Day)	15 PAGE COUNT
Scientific No. 7	FROM 10/87 TO 6/88	1988 June	68

16 SUPPLEMENTARY NOTATION
*This work was partially accomplished under Inhouse Work Unit #7670 15 16
**AFGL/OPA, Hanscom AFB, MA 01731

17 COSATI CODES		
FIELD	GROUP	SUB-GROUP

18 SUBJECT TERMS (Continue on reverse if necessary and identify by block number)
Mie Theory, Scattering Approximations, Aerosol Modeling

19 ABSTRACT (Continue on reverse if necessary and identify by block number)

This report examines how the scattering properties of spheres can be calculated without using Mie theory. Specifically, the scheme of ray optics is used to develop software that calculates the phase matrix elements of polydisperse spheres in geometrical optics limit. (Ray optics works well for size parameters greater than 400, and becomes more accurate for particles containing significant absorption.) In addition, this report examines a collection of numerical algorithms, developed by Nussenzveig and Wiscombe , that use complex angular momentum theory to obtain the efficiency factors for Mie scattering. Although accurate for size parameters greater than 20, it is shown that these algorithms are only computationally efficient for size parameters greater than 500. Finally, this report establishes regions of validity for other
(over)

20 DISTRIBUTION / AVAILABILITY OF ABSTRACT	21 ABSTRACT SECURITY CLASSIFICATION
☐ UNCLASSIFIED/UNLIMITED ☐ SAME AS RPT ☐ DTIC USERS	Unclassified
22a NAME OF RESPONSIBLE INDIVIDUAL Eric P. Shettle	22b TELEPHONE (Include Area Code) 617-377-3665 — 22c OFFICE SYMBOL AFGL/OPA

DD FORM 1473, 84 MAR — 83 APR edition may be used until exhausted. All other editions are obsolete.

SECURITY CLASSIFICATION OF THIS PAGE

19. Abstract (continued)

approximations to the Mie efficiency factors which exist in the scientific literature. It is shown that existing approximations can give reasonable estimates for the extinction efficiency for most size parameters and complex indices of refraction. On the otherhand, the approximations for the absorption efficiency are much less accurate.

Table of Contents

1. INTRODUCTION 1

1.1 Organization of the Report 1

2. THE USE OF RAY OPTICS TO OBTAIN THE SCATTERING MATRIX ELEMENTS FOR A SPHERE 3

2.1 Overview 3
2.2 Fraunhofer Diffraction 5
2.3 Geometrical Optics 5
2.4 Relationship Between Gain And The Phase Matrix Elements 8
2.5 Ray Optics Subroutine 9
2.6 Sample Calculations Using RAYOPT 13

3. CALCULATING MIE EFFICIENCY FACTORS WITH COMPLEX ANGULAR MOMENTUM THEORY 21

3.1 Overview 21
3.2 Software 22
3.3 Timing Comparisons with Mie Theory 22
3.4 A Singularity in the Expression for Q_{ext} 27

4. OTHER APPROXIMATIONS FOR Q_{ext} AND Q_{abs} 30

4.1 Approximations That Were Investigated 30
4.2 Comparison Scheme 31
4.2.1 Realm of Comparison 31
4.2.2 Smoothing Function 31

Table of Contents

4.2.3 Percent Error Contour Plots 34
4.3 Results 34
4.3.1 Regions of Validity for the Extinction Approximations 34
4.3.2 Regions of Validity for the Absorption Approximations 41

5. SUMMARY AND CONCLUSIONS 52

REFERENCES 53

APPENDIX A: EQUATIONS FOR THE VARIOUS MIE APPROXIMATIONS INVESTIGATED IN THIS REPORT A-1

Illustrations

1. Path of a Light Ray According to Geometrical Optics, Where p Is the Order of the Ray 6

2. Flow Diagram of the Subroutine RAYOPT 11

3. Recalculation of Figure 1 of Liou and Hansen[2], Angular Gain for Geometrical Optics using RAYOPT 13

4. Recalculation of Figure 2 of Liou and Hansen[2], Degree of Polarization for Geometrical Optics using RAYOPT 14

5. Values of (a) i_1, (b) i_2 and (c) i_3 for Ray Optics and Mie Theory Where There Is No Absorption Within the Particle 16

6. Values of (a) i_1, (b) i_2 and (c) i_3 for Ray Optics and Mie Theory Where There Is Absorption Within the Particle 18

7. Computation Time for Mie Theory (in CPU seconds) as a Function of Size Parameter and the Imaginary Part of the Index of Refraction 23

Illustrations

8. Computation Time for Complex Angular Momentum Theory (in CPU seconds) as a Function of Size Parameter and the Imaginary Part of the Index of Refraction 25

9. Comparison of the Computation Times for Complex Angular Momentum Theory Against Those for Mie Theory 26

10. Percent Errors in Q_{ext} for Complex Angular Momentum Theory for (a) n = 2.50 and (b) n = 3.00 28

11. Mie Theory Calculations of Q_{sct} Showing the Interference and Ripple Structure as a Function of Size Parameter and k for Fixed n (= 1.33) 35

12. Percent Errors in Q_{ext} for the Approximation of (a) Rayleigh, (b) Wiscombe, (c) Deirmendjian, (d) Ackerman and Stephens, and (e) Nussenzveig and Wiscombe for n = 1.54 36

13. Regions of Validity for the Mie Approximations for Q_{ext} 42

14. Percent Errors in Q_{abs} for the Approximation of (a) Rayleigh, (b) Wiscombe, (c) Deirmendjian, (d) Ackerman and Stephens, (e) Nussenzveig and Wiscombe, (f) Bohren and Nevitt, and (g) Levine for n = 1.54 43

15. Regions of Validity for the Mie Approximations for Q_{abs} 51

Tables

1. Input Parameters For RAYOPT 10

2. Important Variables and Functions in RAYOPT 12

3. Summary of the Approximations That Were Investigated 32

4. Particle Characteristics That Were Investigated 33

Preface

We wish to thank Warren Wiscombe of NASA/GSFC for providing us with a copy of the FORTRAN programs that implement the complex angular momentum algorithms developed by Nussenzveig and himself, as discussed in Chapter 3 of this report.

1. INTRODUCTION

Mie theory provides a means of calculating the absorption and scattering of electromagnetic radiation by spheres of any size compared with the wavelength. Although exact, performing full Mie theory calculations is often cumbersome: it requires an excessive amount of numerical storage space and computer time, especially when the particles are large compared with the wavelength. Under certain circumstances however, it is possible to obtain a reasonable estimate of the scattering and absorption properties of spheres without resorting to detailed Mie theory calculations. These alternative approaches to exact Mie theory calculations are useful provided the user realizes their limitations.

The regions of validity for Mie approximations are usually characterized in terms of the size parameter, $X = 2\pi r/\lambda$, where r is the radius of the particle and λ is the wavelength of the impinging radiation. Unfortunately, the use of an approximation over Mie theory is not a clearcut decision; that is, the accuracy of most approximations depend not only on X, but to some extent on the complex index of refraction of the particle, $m = n + ik$. Also the user must consider the degree of accuracy required for his or her particular problem.

1.1 Organization of the Report

It is the aim of this report to explore some of the alternatives to Mie theory and to access their ranges of

applicability. Chapter 2 discusses the use of ray optics to obtain the phase matrix elements of a sphere that is large compared with the wavelength. Chapter 3 discusses the use of complex angular momentum theory to calculate the efficiency factors for extinction, absorption and radiation pressure. Chapter 4 compares various Mie approximations in the scientific literature and assesses their regions of validity. Chapter 5 summarizes the main results of this report. For reference, Appendix A gives the equations for the various Mie approximations investigated in this report.

2. THE USE OF RAY OPTICS TO OBTAIN THE SCATTERING MATRIX ELEMENTS FOR A SPHERE

2.1 Overview

The angular scattering properties of spheres can be calculated using the scheme of ray optics (van de Hulst[1] and Liou and Hansen[2]) provided four conditions are satisfied:

1) the size parameter is much greater than one

2) the real part of the index of refraction is greater than one

3) the user is interested in the scattering pattern for a small spread of particle sizes

4) the far field scattering pattern is desired.

In ray optics, incident radiation is treated as localized rays whose encounters with the particle are governed by the laws of reflection and refraction for geometrical optics. The localized rays can be reflected externally or can enter the particle where they are either absorbed or internally reflected a number of times before exiting. Also, light rays passing very close to the particle are affected by Fraunhofer diffraction. Thus the total intensity at a particular scattering angle is equal to the contribution from Fraunhofer diffraction, plus that for rays emerging from the particle after reflection and refraction.

---

1. van de Hulst, H. C. (1957) Light Scattering by Small Particles, Wiley, Inc., New York, 470 pp.

2. Liou, K., and Hansen, J. E. (1971) Intensity and polarization for single scattering by polydisperse spheres: A comparison of ray optics and Mie theory, J. Atmos. Sci. 28:995-1004.

(Strictly speaking it is not correct to simply add the intensities of the separate rays. For a single particle, emergent rays interfere with each other because of phase changes caused by external and internal reflection, and by differing optical paths. These interference effects lead to rapid oscillations in the scattered intensity as a function of scattering angle which can only be predicted by Mie theory. However if a small spread of particle sizes is considered, any phase effects are averaged out when integrating over the spread of particle sizes.)

In ray optics, the gain, G, is used to describe the relative scattered intensity as a function of scattering angle. It represents the ratio of scattered intensity to that which would exist if it were scattered isotropically and conservatively[2]. Thus the gain is defined such that

$$w_o = \frac{\int G(\Omega)\, d\Omega}{\int d\Omega} = \frac{1}{4\pi} \int G(\Omega)\, d\Omega \qquad (1)$$

where Ω is the solid angle and w_o, the single scattering albedo, is the ratio of the scattered energy to that scattered and absorbed by the particles.

Below the equations governing ray optics are presented. These equations are essentially the same as those found in van de Hulst[1] and in Liou and Hansen[2]. Next, a Fortran subroutine called RAYOPT is described which determines the angular dependent phase matrix elements i_1, i_2, i_3 and i_4. These matrix elements relate the polarization and the amplitude of the incident field to that of the scattered field.

The results from RAYOPT are then verified against those from Liou and Hansen, and from full Mie theory.

2.2 Fraunhofer Diffraction

Diffraction of the incident beam occurs because the wavefront is partially obstructed as it passes very close to the particle. For spheres, the gain as a function of scattering angle resulting from diffraction is given by

$$G_1^F(\theta,X) = G_2^F(\theta,X) = 2X^2\left[\frac{J_1(X\sin\theta)}{X\sin\theta}\right]^2 \qquad (2)$$

where the superscript F denotes the gain due to Fraunhofer diffraction, J_1 is the first order Bessel function and the subscripts 1 and 2 refer to the gain components perpendicular and parallel, respectively, to a particular scattering plane. The diffracted pattern is radially symmetric about the forward direction and becomes more concentrated in the forward direction as the size parameter increases. For the case when $\theta = 0$, $G_1^F(0,X) = G_2^F(0,X) = 0.5X^2$.

2.3 Geometrical Optics

The geometry of the problem is given in Figure 1. The angle between an incident ray and the tangent of the local particle surface is denoted by τ. For grazing incidence, τ equals 0 degrees; for central incidence, τ equals 90 degrees. As an incident ray encounters the particle, some of its energy is externally reflected while the rest enters the particle. The ratio of externally reflected energy to the

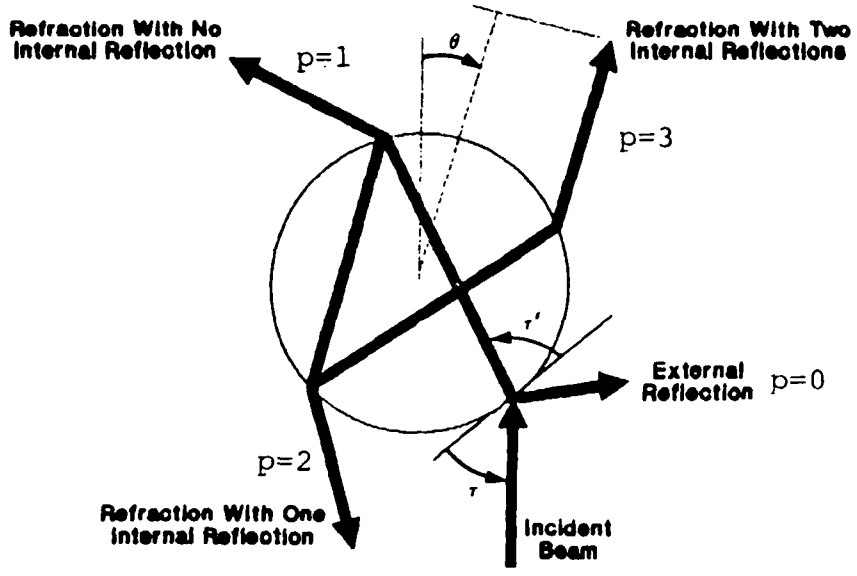

Figure 1. Path of a Light Ray According to Geometrical Optics, Where p Is the Order of the Ray (see Eq. 6)

incident energy is equal to the squares of the Fresnel reflection coefficients, r_1 and r_2:

$$|r_1|^2 = \left| \frac{\sin\tau - m \sin\tau'}{\sin\tau + m \sin\tau'} \right|^2 \qquad (3)$$

and

$$|r_2|^2 = \left| \frac{m \sin\tau - \sin\tau'}{m \sin\tau + \sin\tau'} \right|^2 \qquad (4)$$

where τ' is the direction of the ray upon entering the particle. The angle τ' is related to the incident angle, τ, through Snell's law

$$\cos\tau' = \cos\tau/n \quad . \qquad (5)$$

Because energy is conserved, the energy entering the particle must either be absorbed or emerge after any number of

internal reflections. For a nonabsorbing particle, the fraction of energy emerging after refraction with no internal reflection is equal to $(1-|r_{1,2}|^2)^2$; after one internal reflection, it is $|r_{1,2}|^2(1-|r_{1,2}|^2)^2$, etc. Here it is convenient to define

$$e_{1,2}^2 = \begin{cases} |r_{1,2}|^2 & \text{for } p = 0 \\ (1-|r_{1,2}|^2)^2(|r_{1,2}|^2)^{p-1} & \text{for } p \geq 1 \end{cases} \tag{6}$$

where $p = 0$ means external reflection and $p \geq 1$ means refraction plus $p-1$ internal reflections (see Fig. 1). The gain for geometrical optics, as given by Liou and Hansen[2], is then

$$G^{(p)}_{1,2}(\theta,X) = 2e^2_{1,2}D \exp(-4X\ k\ p \sin\tau'), \tag{7}$$

where D is the divergence, defined as

$$D = \frac{\sin\tau\cos\tau}{\sin\theta\left|\frac{d\theta}{d\tau}\right|} \tag{8}$$

and

$$\frac{d\theta}{d\tau} = 2 - 2p\,\frac{\tan\tau}{\tan\tau'} \tag{9}$$

In Eq. 7, the exponential term accounts for absorption within the particle. The total gain at a particular scattering angle is then

$$G_{1,2}(\theta,X) = G^F_{1,2} + \sum_{p=0}^{N} G^{(p)}_{1,2} \tag{10}$$

where in practice, a value of 3 for N is sufficient to account for most of the energy scattered by geometrical optics.

2.4 Relationship Between Gain And The Phase Matrix Elements

The angular dependent phase matrix elements relate the polarization and amplitude of the scattered field to the incident field. In the work of Blattner[3], the incident and scattered fields are described by the parameters I_1, I_2, U and V which are similar to, but not the same as, the Stokes parameters. For a spherical scatterer, the scattered field (s subscript) is related to the incident field (o subscript) through the amplitude scattering matrix

$$\begin{vmatrix} I_{s1} \\ I_{s2} \\ U_s \\ V_s \end{vmatrix} = \frac{\lambda^2}{4\pi^2 R^2} \begin{vmatrix} i_1 & 0 & 0 & 0 \\ 0 & i_2 & 0 & 0 \\ 0 & 0 & i_3 & i_4 \\ 0 & 0 & -i_4 & i_3 \end{vmatrix} \begin{vmatrix} I_{o1} \\ I_{o2} \\ U_o \\ V_o \end{vmatrix} \qquad (11)$$

where R is the distance from the scatterer to the observer and i_1, i_2, i_3 and i_4 are the angular dependent scattering matrix elements defined as

$$\begin{aligned} i_1 &= c|S_1|^2 \\ i_2 &= c|S_2|^2 \\ i_3 &= c\ \mathrm{Re}\{S_1 S_2^*\} \\ i_4 &= -c\ \mathrm{Im}\{S_1 S_2^*\} \end{aligned} \qquad (12)$$

---

3. Blattner, W. (1972) Utilization instructions for operation of the Mie programs on the CDC-6600 computer at AFCRL, F19628-70-C-0156, Research Note, RRA-N7240, Radiation Research Associates, Inc., Fort Worth, Texas.

where S_1 and S_2 are the familar complex amplitude functions and c is a normalization constant such that

$$1 = \int i_1(\Omega) d\Omega \quad . \tag{13}$$

Comparing Equations 1 and 13 suggests that

$$\begin{aligned} i_1 &= G_1/4\pi w_o \\ i_2 &= G_2/4\pi w_o \\ i_3 &= (G_1 G_2)^{1/2}/4\pi w_o \\ i_4 &= 0 \end{aligned} \tag{14}$$

2.5 Ray Optics Subroutine

A subroutine called RAYOPT has been developed to determine the phase matrix elements i_1, i_2, i_3 and i_4 at user specified scattering angles. The inputs to the subroutine are listed in Table 1. A flow diagram for RAYOPT is given in Figure 2 and a brief description of the important variables and functions is given in Table 2.

For geometrical optics, RAYOPT determines the gains at the user scattering angles in the following manner. With p held fixed, the total deviation of a ray from its original path, θ', is computed for incident angles, τ, between 0 and 90 degrees in steps of 0.5 degrees where

$$\theta' = 2\tau - 2p\tau' \quad . \tag{15}$$

Next, each user scattering angle is transformed so that it also represents the total deviation of a ray from its original path. This deviation is then compared with the devia-

Table 1. Input Parameters for RAYOPT

VARIABLE	DESCRIPTION
NP	Maximum Value for p When Performing the Ray Tracing
NTHETA	Number Of User Scattering Angles. The Maximum is 150
PM	Complex Index of Refraction of the Particle. The Imaginary Part Is Positive
THET(150)	Array Containing the User Scattering Angles
WO	Single Scattering Albedo of the Particle
X	Size Parameter

tions for known incident angles to determine what incident angles yield emergent rays at a user scattering angle. When a user scattering angle falls between two values of θ', the incident angle is obtained by means of a linear interpolation. With the incident angle now known, the gain at the user scattering angle is calculated using Eqs. 3 - 9.

Before computing the gain, RAYOPT checks to make sure the incident angle does not lead to either a rainbow, i.e. $d\theta/d\tau \rightarrow 0$, or a glory, i.e. $\theta = 180$ and $\sin\theta = 0$. (The scheme of ray optics predicts infinite intensities at these angles, see Eq. 8.) If a rainbow or glory angle is found, the gain calculation is performed for an incident angle given by $\tau = \tau - 2$ degrees. The resulting gain is then used unless it is still excessively large (>100); in that case, the gain

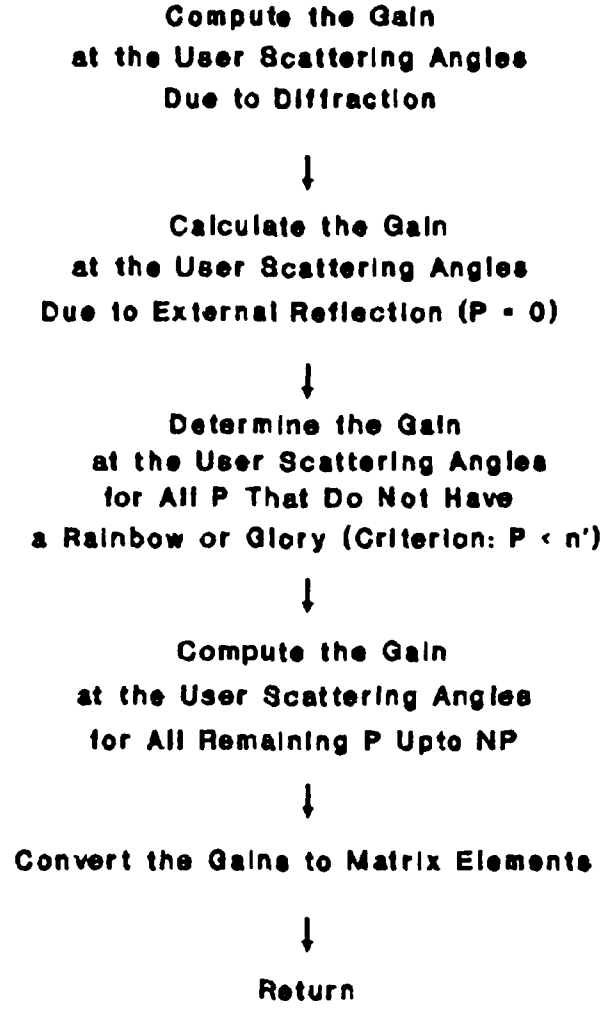

Figure 2. Flow Diagram of the Subroutine RAYOPT

Table 2. Important Variables and Functions in RAYOPT

PARAMETER	DESCRIPTION
GAINP	Function That Returns the Gain for a Given Incident Angle and p
GAIN1(150), GAIN2(150)	Keeps a Running Total of the Gains at the User Scattering Angles
GDIFF(150)	Gains at the User Scattering Angles Due To Fraunhofer Diffraction
J1	Function That Returns The Bessel Function Of The First Kind
PNAUT	Maximum Value of p that Does Not Have a Rainbow or Glory
RENT1(150), RENT2(150) ENT3(150), ENT4(150)	Angular Dependent Matrix Elements i_1, i_2, i_3 and i_4 Respectively
TAU	Angle of An Incident Ray With Respect To The Particle Surface
THETPR(181)	Array Containing the Total Deviation of Emergent Rays for Incident Rays between 0 and 90 degrees in Steps of 0.5 degrees

is set equal to 100. The gain calculations are simplified for $p \leq n$ because they do not contain rainbows or glorys. These values of p are done first in RAYOPT where the amount of computer time is reduced significantly. Finally for central incidence, where τ is 90 degrees and θ is 0 degrees, the gain equals $G^{p}_{1,2} = 0.5(e_{1,2}{}^{2}/(1-p/n)^{2})\exp(-4X\ k\ p)$.

2.6 Sample Calculations Using RAYOPT

To ensure that RAYOPT is working properly, a series of calculations have been performed and compared with those from other researchers. Figures 3 and 4 duplicate Figures 1

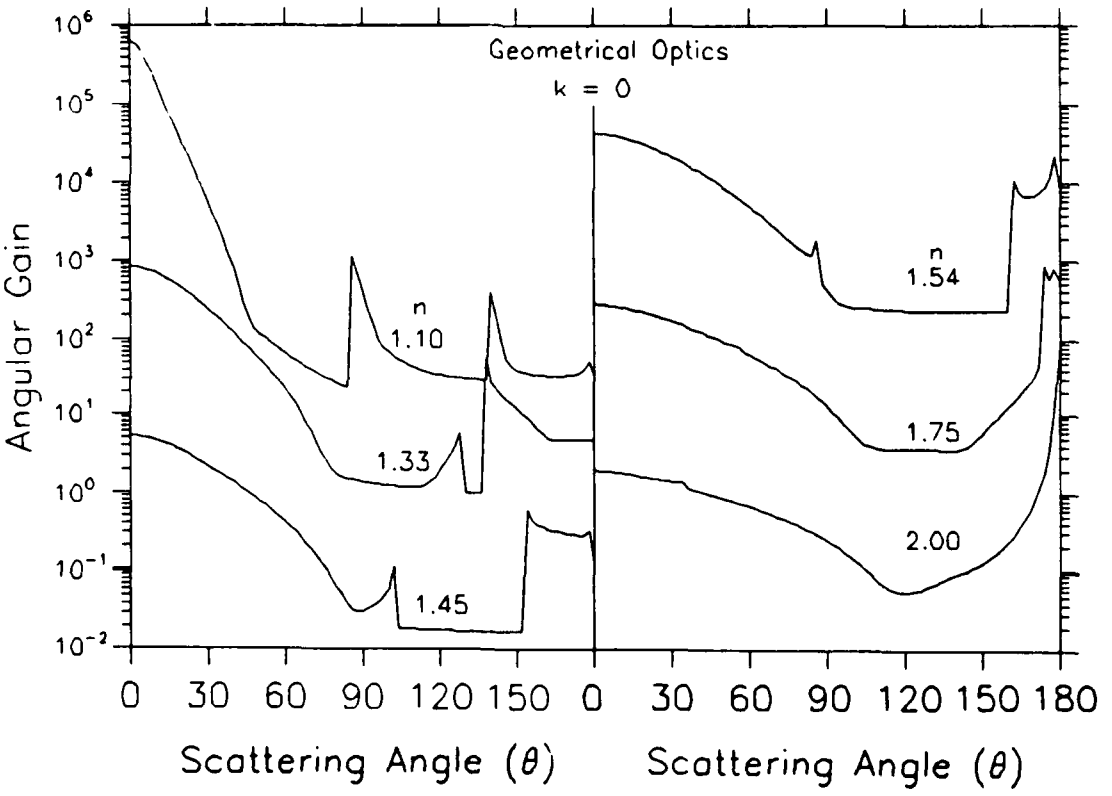

Figure 3. Recalculation of Figure 1 of Liou and Hansen[2], Angular Gain for Geometrical Optics using RAYOPT. The Vertical Scale Applies to the Lowermost Curves (n = 1.45 and 2.00) while the Other Curves Are Displaced Upwards by Factors of 10^{2}

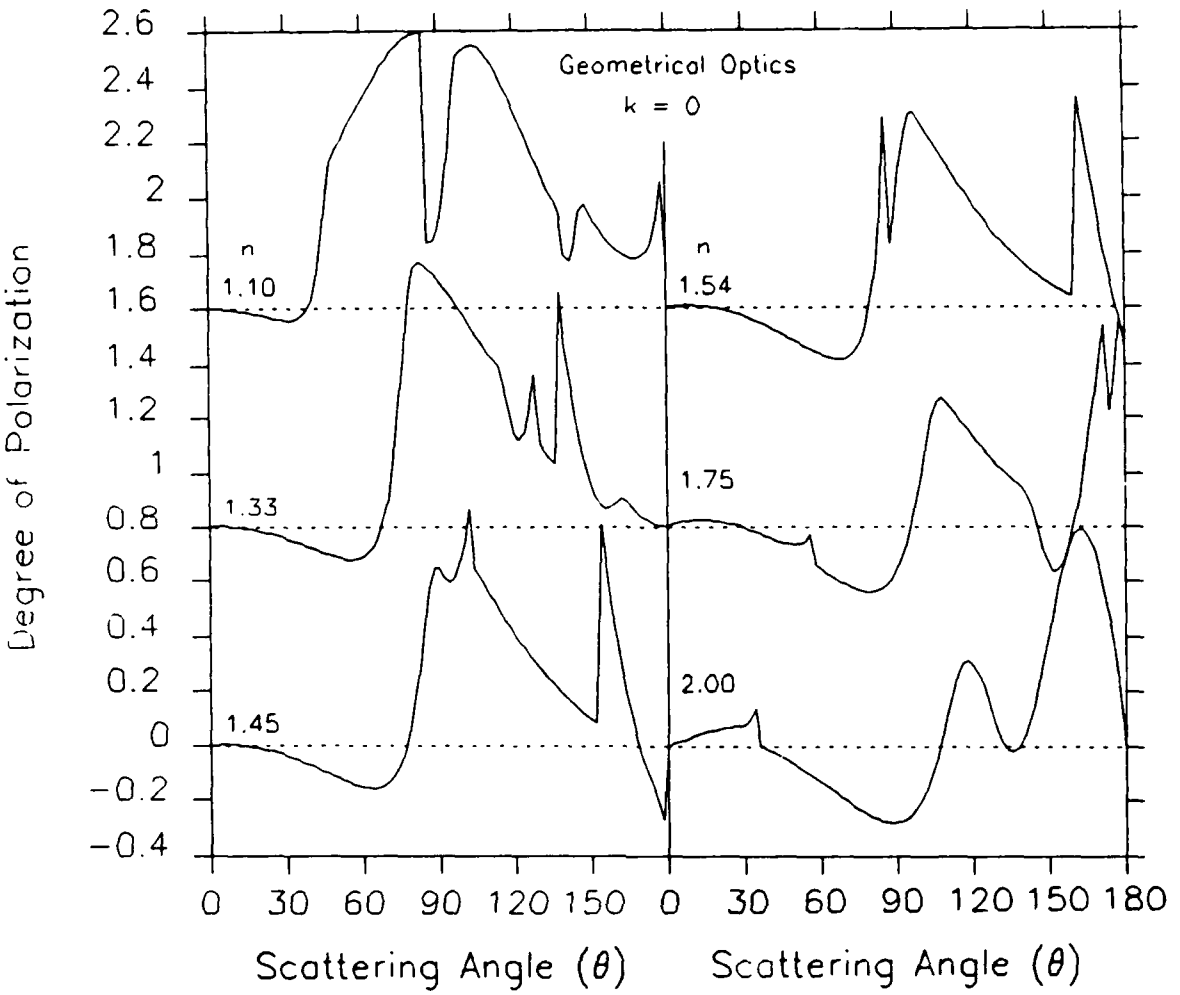

Figure 4. Recalculation of Figure 2 of Liou and Hansen[2], Degree of Polarization for Geometrical Optics using RAYOPT. The Vertical Scale Applies to the Lowermost Curves (n = 1.45 and 2.00) while the Other Curves Are Displaced Upwards by 0.8

and 2 of Liou and Hansen[2]. There is complete agreement except in some instances at the rainbow and glory angles: Liou and Hansen did not say how they dealt with these angles.

Figures 5 and 6 give comparisons between ray optics and Mie theory for the matrix elements i_1, i_2 and i_3. Figure 5 represents the scattering by a particle with an index of refraction of 1.33 + 0.0i while in Figure 6, an index of refraction of 1.54 + 0.01i has been used. In both figures, the matrix elements for ray optics represent a size parameter of 400. When performing the Mie calculations, it was necessary to use a particle number density distribution, N(r), described by a log-normal distribution because interference effects lead to rapid oscillations in the angular scattering pattern of a single sphere. This analytical formulation is given by

$$\frac{dN(r)}{d\log(r)} = \frac{N_o}{(2\pi)^{1/2}\log\sigma} \exp\left[-\left(\frac{\log(r/r_o)}{2\log\sigma}\right)^2\right] \qquad (16)$$

where r_o, σ and N_o are the geometric mean radius, geometric standard deviation and total number of particles respectively. In Figures 5 and 6, an r_o of 63.66 micrometers, σ of 0.1, and N_o of 1 particle cm^{-1} have been used. The value for r_o was chosen because it converts to a size parameter of 400 for 1 micrometer radiation. The range of the Mie calculations was from 50 to 100 micrometers.

Figure 5(a) shows good agreement between the values of i_1 for ray optics and Mie theory except for the rainbow region from 130 to 140 degrees and at 180 degrees. The peak

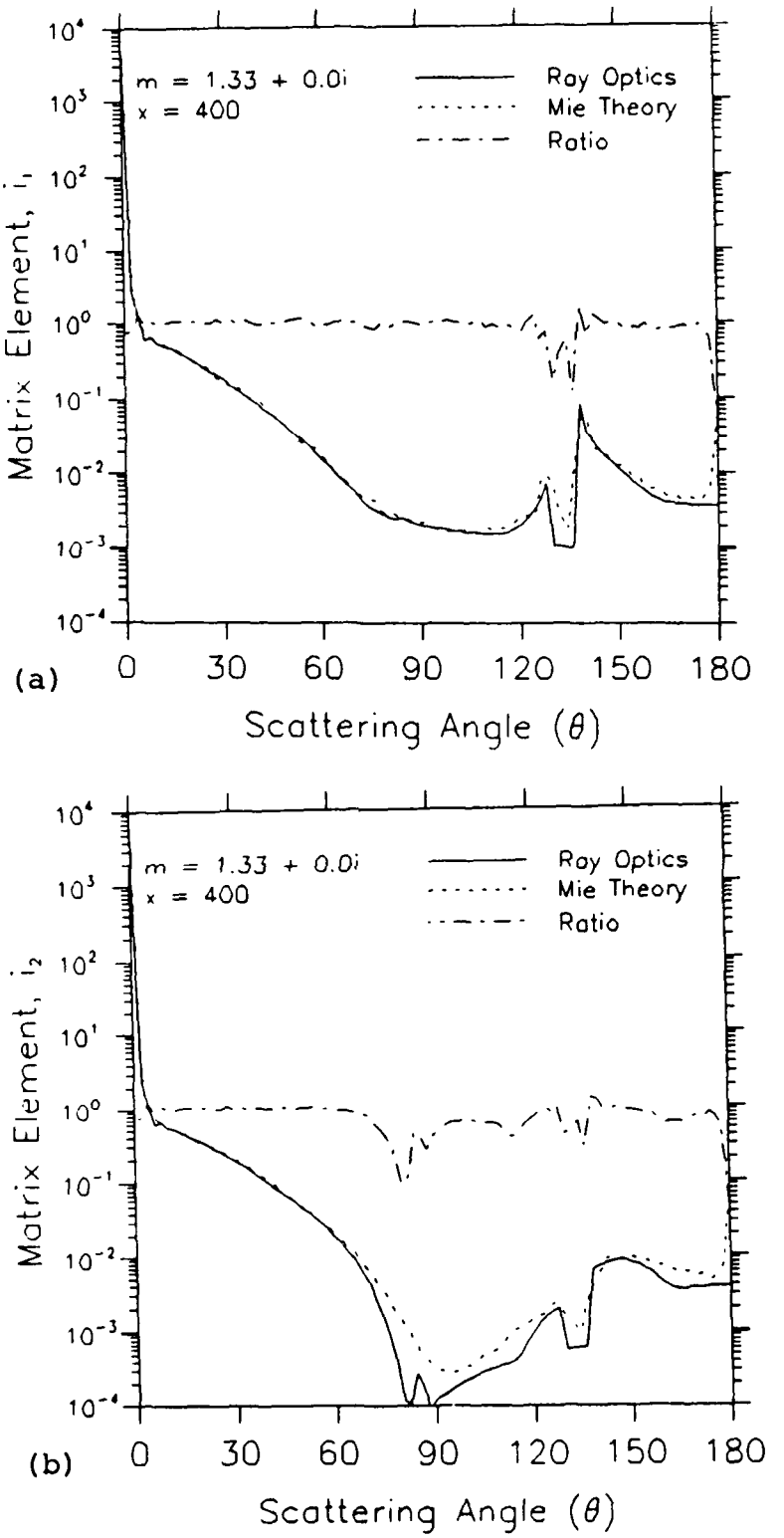

Figure 5. Values of (a) i_1, (b) i_2 for Ray Optics and Mie Theory Where There Is No Absorption Within the Particle

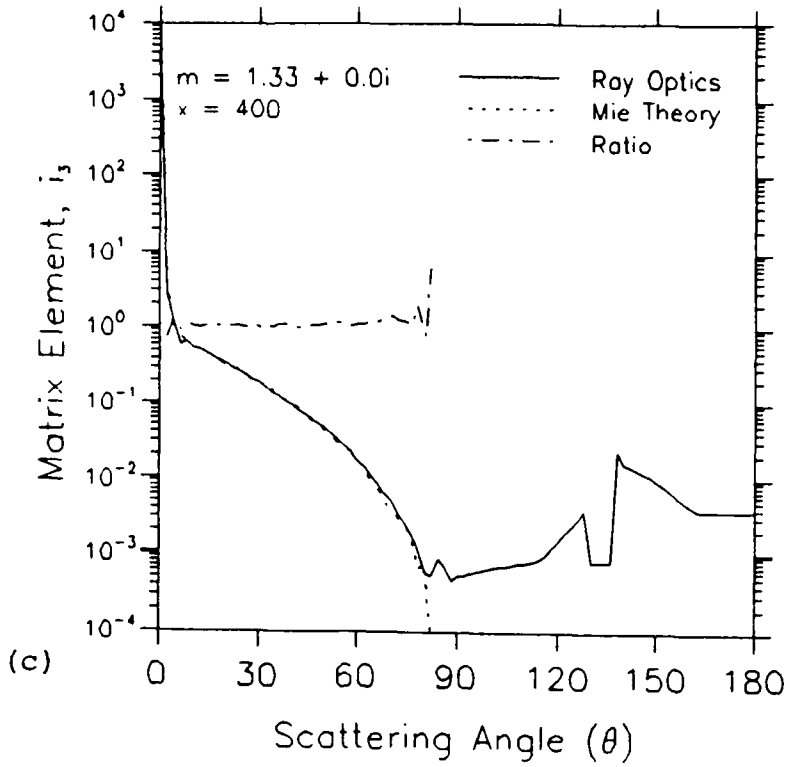

Figure 5. (continued) Values of (c) i_3 for Ray Optics and Mie Theory Where There Is No Absorption Within the Particle. In (c) the Values Beyond About 80 Degrees Are Not Plotted Because i_3 for Mie Theory Is Negative

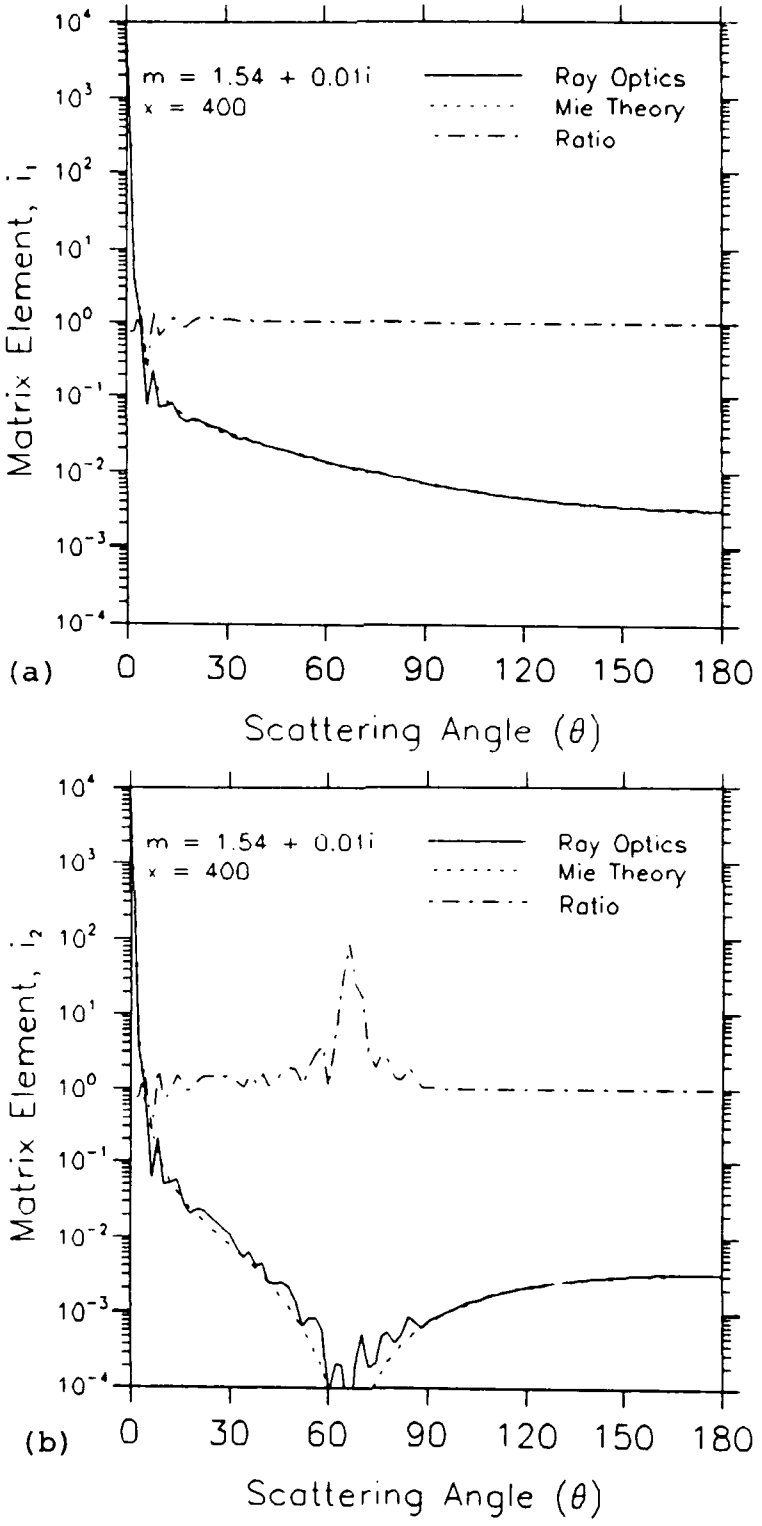

Figure 6. Values of (a) i_1, (b) i_2 for Ray Optics and Mie Theory Where There Is Absorption Within the Particle

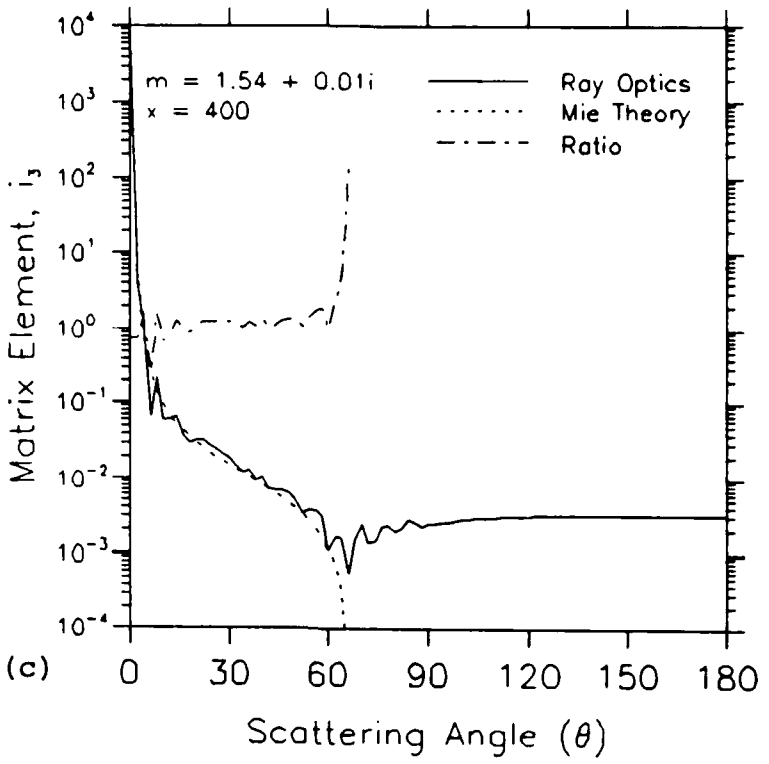

Figure 6. (continued) Values of (c) i_3 for Ray Optics and Mie Theory Where There Is Absorption Within the Particle. In (c) the Values Beyond About 70 Degrees Are Not Plotted Because i_3 for Mie Theory Is Negative

at 180 degrees for Mie theory is related to the familiar glory phenomenon. Ray optics does not predict the glory and here lies one of its major weaknesses. Figure 5(b) suggests only fair agreement between the values of i_2 for ray optics and Mie theory. In Figure 5(c), the values of i_3 for ray optics are close to those for Mie theory provided the scattering angle is less than 80 degrees. Beyond this angle however, ray optics cannot be used in place of Mie theory because i_3 for Mie theory is negative. This limitation of ray optics is not as severe as it may appear since $|i_3|$ is small beyond 80 degrees.

Figures 6(a) and 6(b) show better general agreement between Mie theory and ray optics except near the diffraction peak. The improved accuracy of ray optics can be attributed to the absorption within the particle which eliminates the less accurate contributions from $p \geq 1$. However discrepancies still exist in the values of i_2 for scattering angles between 60 and 80 degrees. Here, ray optics predicts values for i_2 that are 10 to 100 times greater than Mie theory. In Figure 6(c), the values of i_3 for ray optics are close to those for Mie theory provided the scattering angle is less than 60 degrees. Beyond 60 degrees, Mie theory predicts negative values for i_3.

3. CALCULATING MIE EFFICIENCY FACTORS WITH COMPLEX ANGULAR MOMENTUM THEORY

3.1 Overview

Three parameters often obtained from Mie theory calculations are the efficiency factors for extinction, absorption and radiation pressure which are refered to as Q_{ext}, Q_{abs} and Q_{pr} respectively. Q_{ext} and Q_{abs} are related to the extinction and absorption cross sections, C_{ext} and C_{abs}, by

$$Q_{ext} = \frac{C_{ext}}{A} \tag{17}$$

and

$$Q_{abs} = \frac{C_{abs}}{A} \tag{18}$$

where A is the cross-sectional area of the sphere and the scattering efficiency follows as $Q_{sct} = Q_{ext} - Q_{abs}$. The radiation pressure efficiency, which measures the total rate of momentum transfer to the particle, can be converted to the asymmetry parameter, g, by

$$g = (Q_{ext} - Q_{pr})/Q_{sct} \ . \tag{19}$$

Complex angular momentum theory can be used to determine the Mie efficiency factors of a sphere that is large compared with the wavelength. The governing equations have been developed by Nussenzveig and Wiscombe[4]. (These equations have been replicated in Appendix A due to their ex-

4. Nussenzveig, H. M., and Wiscombe, W. J. (1980) Efficiency factors in Mie scattering, Phys. Rev. Letters, 45: 1490-1494.

treme length.) Nussenzveig and Wiscombe have shown that when compared with exact Mie values, complex angular momentum theory gives relative errors of ~(1-10)% for X = 10 and ~(0.01-0.001)% for X = 1000. The theory does not predict the rapid changes in the values of Q_{ext} and Q_{abs} as a function of size parameter, but this high-frequency "ripple structure" can be ignored in many applications.

3.2 Software

Source code has been obtained from Warren Wiscombe[5] which calculates Q_{ext}, Q_{abs} and Q_{pr} using complex angular momentum theory. The code was written in standard Fortran 77 and therefore, required very few modifications to operate on the AFGL CYBER system. Specifically, to avoid underflow errors, checks have been inserted before calls to the Fortran CEXP function. In addition the ACCUR parameter in the code, which establishes a convergence criterion for numerical integrations, has been changed from 10^{-6} to 10^{-3}. This change was recommended by Warren Wiscombe and acts to speed up the program without a significant loss of accuracy.

3.3 Timing Comparisons with Mie Theory

It is well known that the computation time for Mie calculations is directly proportional to the size parameter. Figure 7 illustrates this clearly where the contours represent CPU times for various size parameters and imaginary indices of refraction. The CPU times were determined using

5. Wiscombe, W. J., private communication.

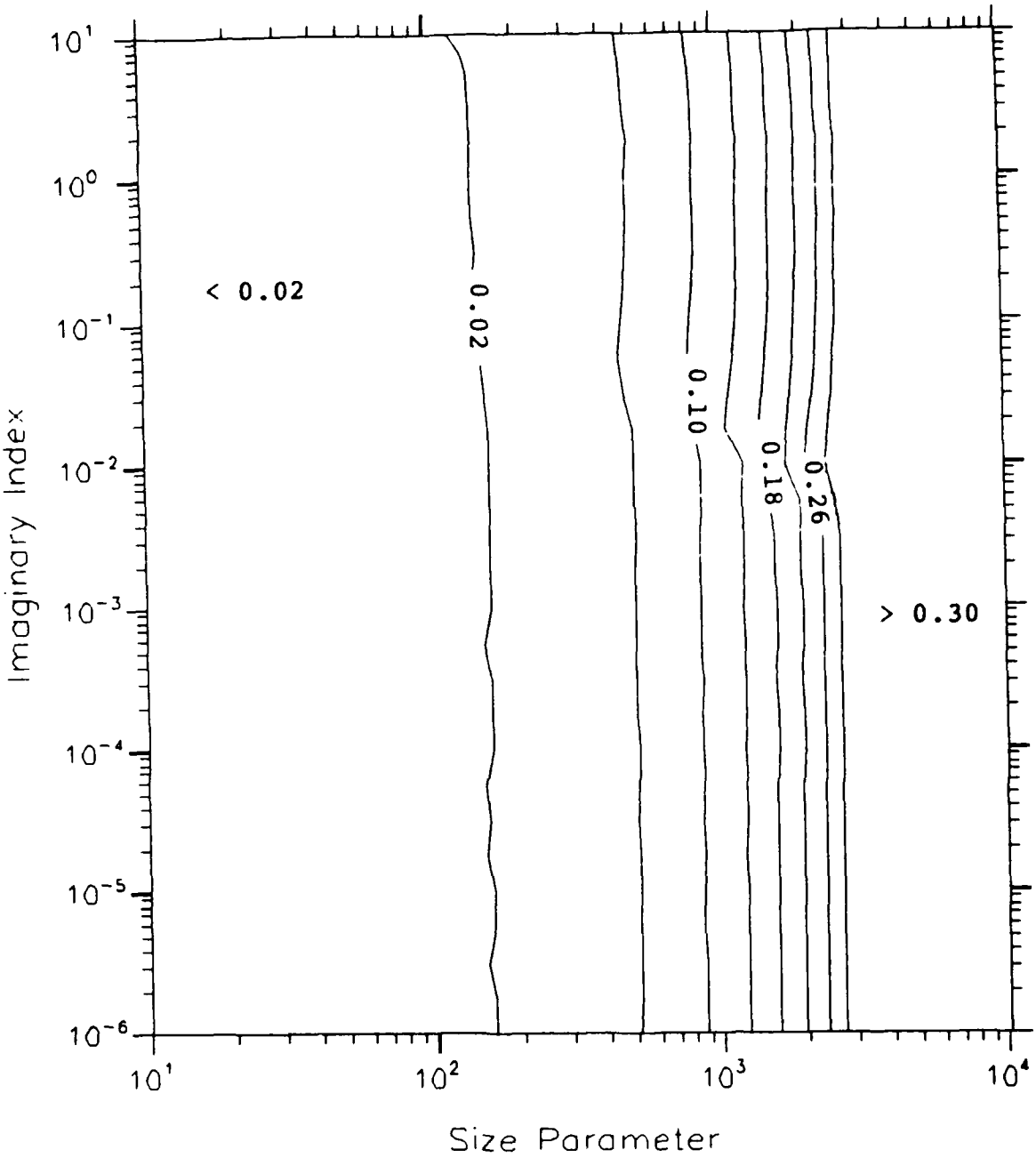

Figure 7. Computation Time for Mie Theory (in CPU seconds) as a Function of Size Parameter and the Imaginary Part of the Index of Refraction

the Fortran SECOND function, available on the AFGL Cyper computer.

For complex angular momentum theory, the expression for Q_{ext} is a "one line" expression that requires very little computer time. On the otherhand, the expressions for Q_{abs} and Q_{pr} involve numerical integrations that require more CPU time. Therefore, a series of timing runs have been performed for a wide range of size parameters and indices of refraction to determine where complex angular momentum theory is faster than Mie theory. In the comparisons, the CPU time for complex angular momentum theory represents the total time required to compute Q_{ext}, Q_{abs} and Q_{pr}. (Q_{ext}, Q_{abs} and Q_{pr} are computed simultaneously during a single Mie run.)

Figure 8 gives CPU times for complex angular momentum theory as a function of size parameter and imaginary index of refraction. The figure suggests that there is broad minima in the CPU time for imaginary indices of ~(0.01-1). Other timing runs indicated that the CPU times were not influenced by the real index of refraction.

Figure 9 compares the CPU times for complex angular momentum theory against those for Mie theory where the comparison is expressed as

$$\log \frac{T_{APX}}{T_{MIE}} \quad . \tag{20}$$

In Figure 9, it can be seen that complex angular momentum theory is faster than Mie theory for size parameters greater

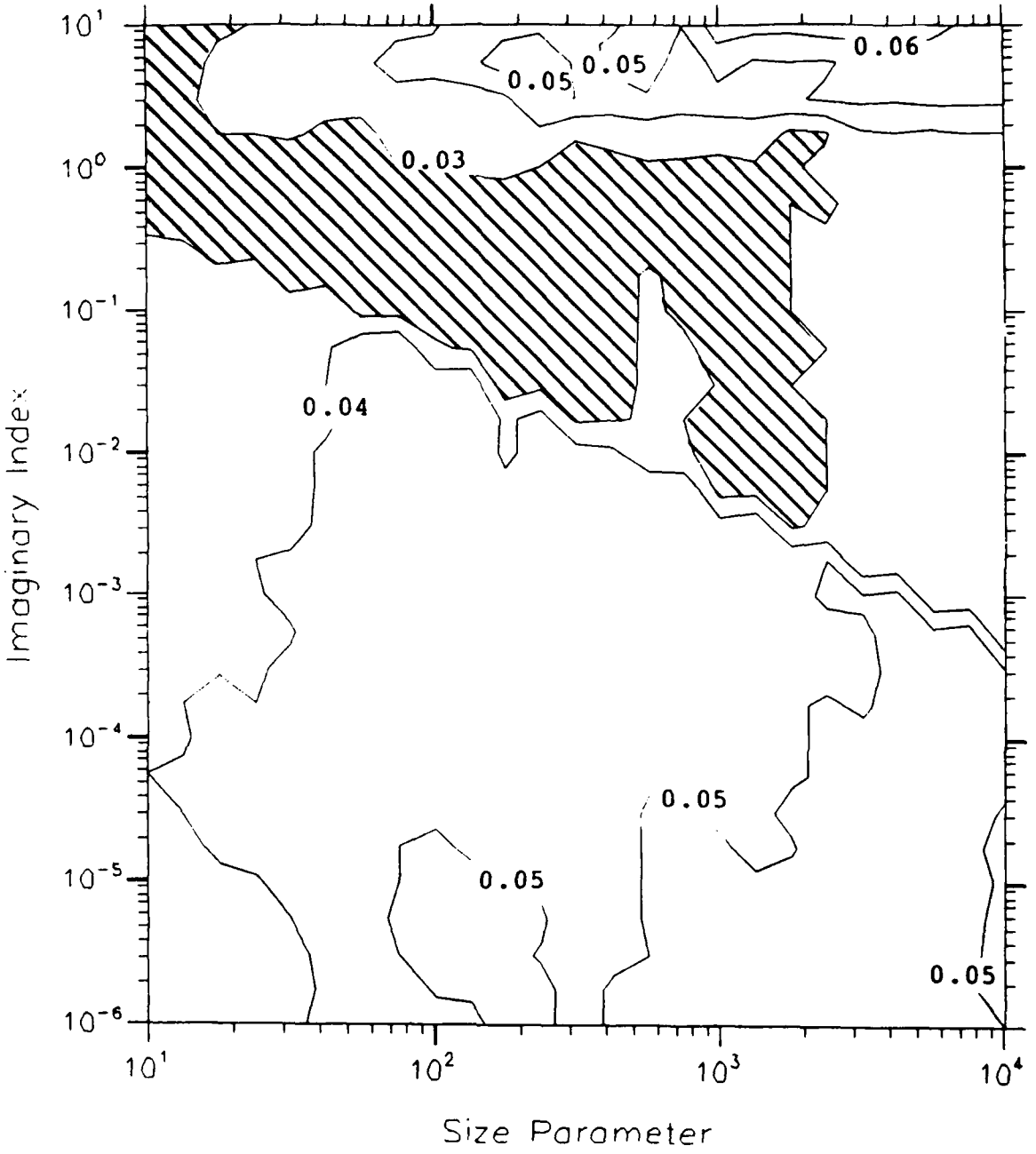

Figure 8. Computation Time for Complex Angular Momentum Theory (in CPU seconds) as a Function of Size Parameter and the Imaginary Part of the Index of Refraction. The Shaded Region Denotes Where the Computation Time Is Less Than 0.03 Seconds

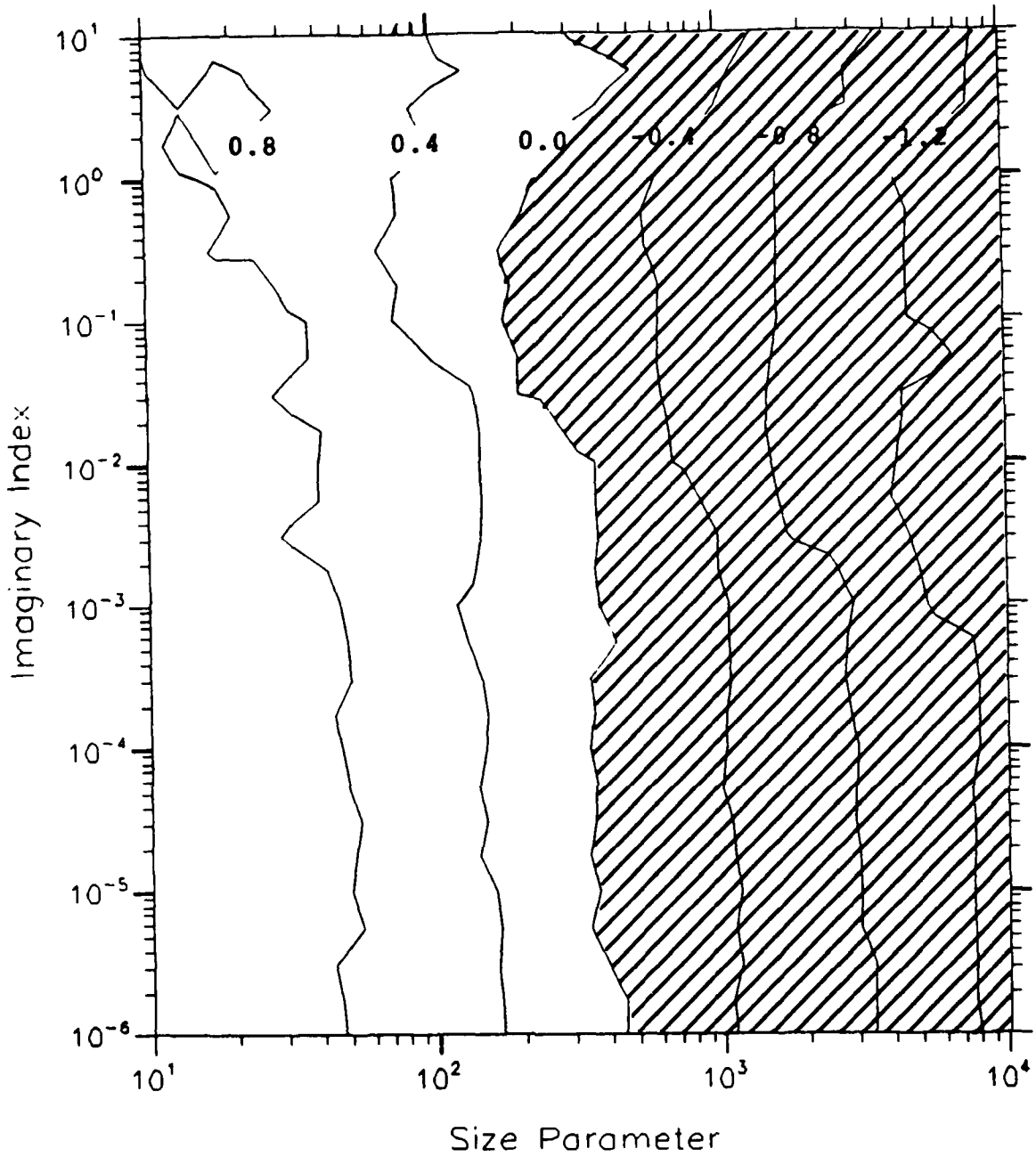

Figure 9. Comparison of the Computation Times for Complex Angular Momentum Theory Against Those for Mie Theory. The Shaded Region Indicates Where Complex Angular Momentum Theory Is Faster Than Mie Theory

than 200 to 500, depending on the imaginary index of refraction. Furthermore, percent errors are generally less than 1% for size parameters greater than 500 so Mie theory can be replaced by complex angular momentum theory without sacrificing accuracy.

3.4 A Singularity in the Expression for Q_{ext}

In the course of testing the source code provided by Warren Wiscombe, it was discovered that a singularity exists for Q_{ext} whenever the imaginary index was less than about 10^{-3} and the real index equals 3, 5, 7... Specifically, this ill-behavior arises from a division by zero in the summation term of Eq. 1 of Nussenzveig and Wiscombe[4]. The extent of the ill-behavior can be seen in Figures 10(a) and 10(b) where percent errors, when compared with Mie theory values, are given for real parts of 2.5 and 3.0. Subsequent testing showed that the expression for Q_{ext} can be used confidently provided

$$|n - n^*| > 0.05 \qquad (21)$$

where $n^* = 3, 5, 7...$

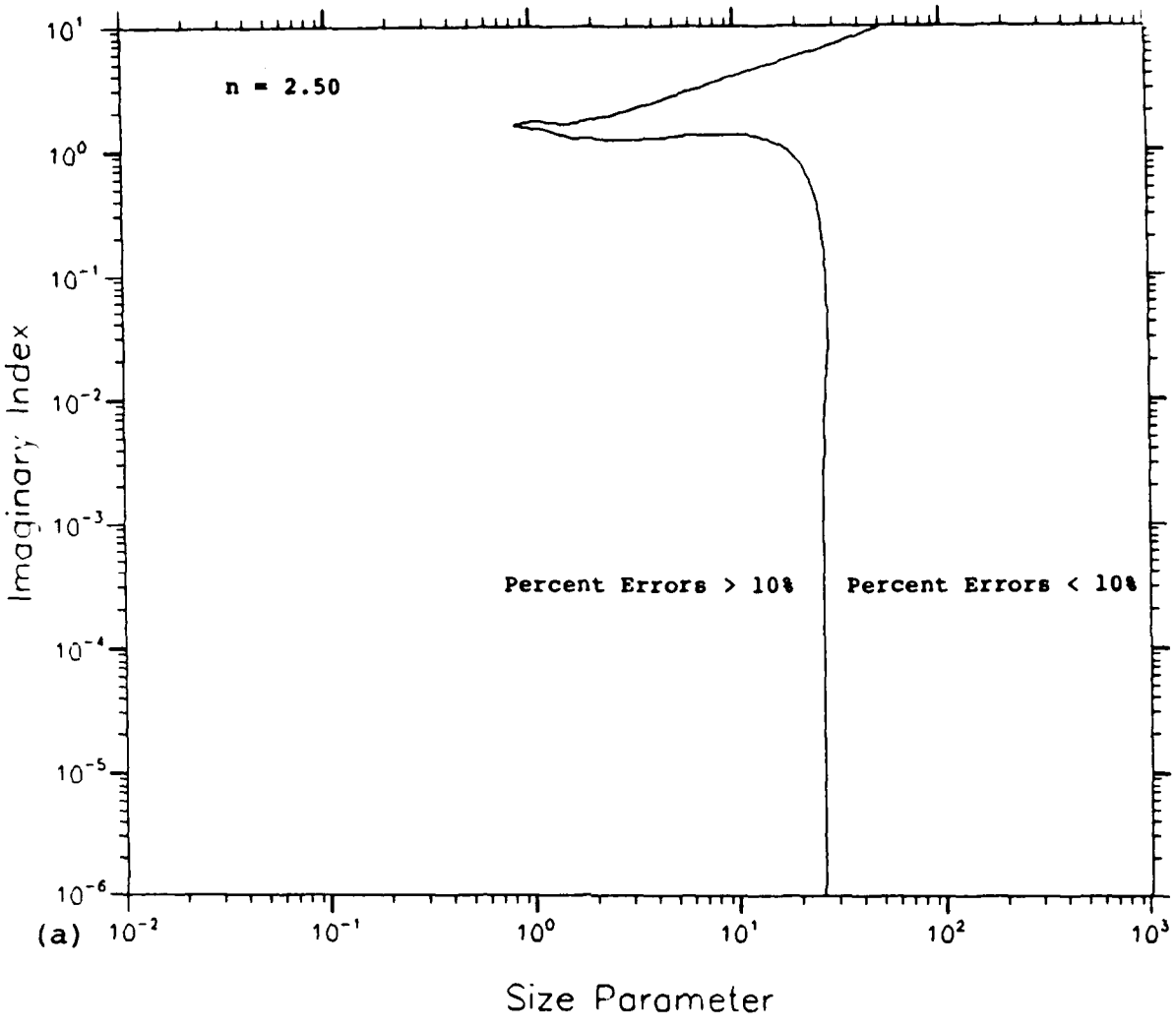

Figure 10. Percent Errors in Q_{ext} for Complex Angular Momentum Theory for (a) n = 2.50

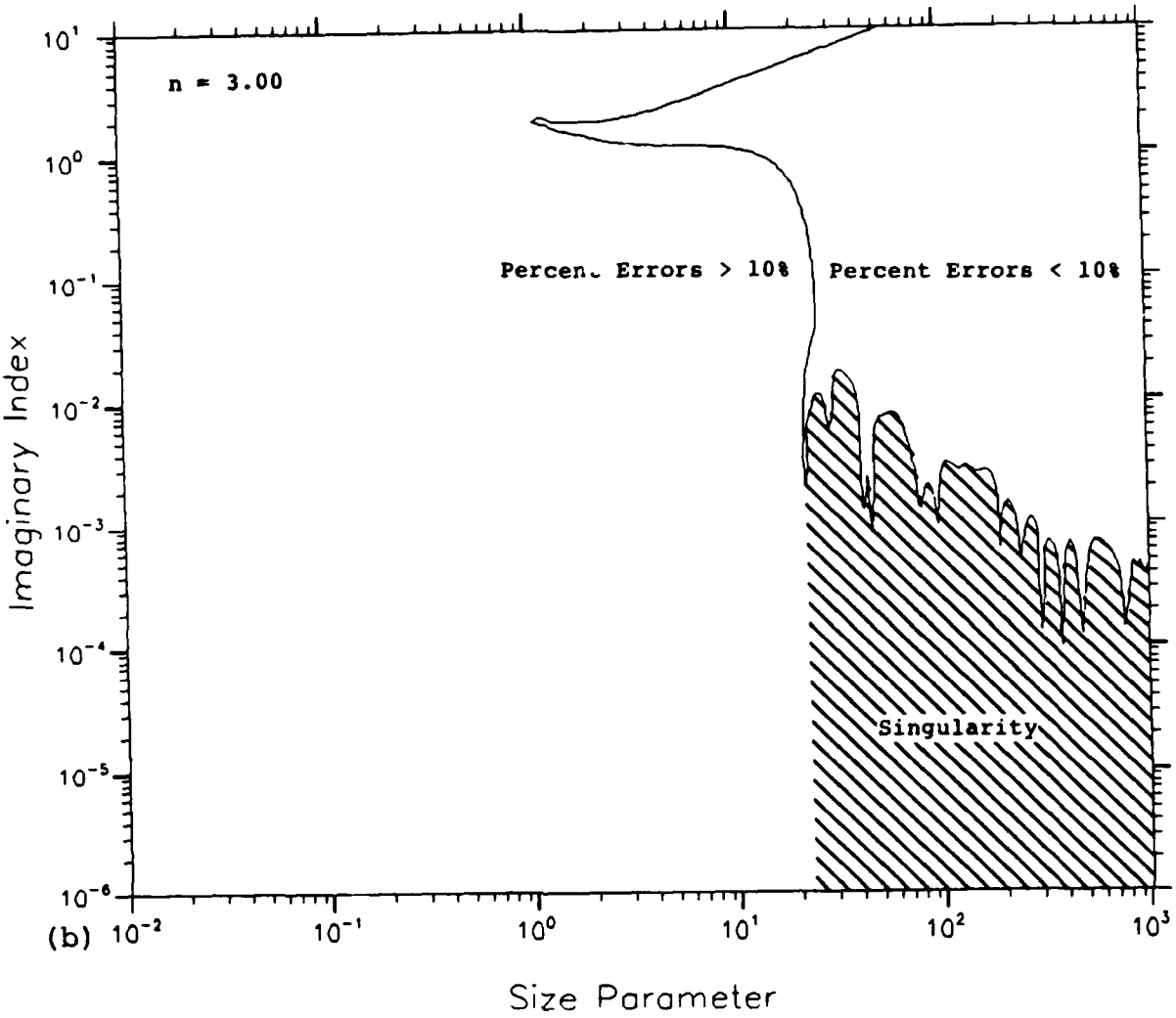

Figure 10. (continued) Percent Errors in Q_{ext} for Complex Angular Momentum Theory for (b) n = 3.00. In (b), the Shaded Region Illustrates the Singularity

4. OTHER APPROXIMATIONS FOR Q_{ext} AND Q_{abs}

This chapter examines various approximations for Q_{ext} and Q_{abs} that are available in the scientific literature. Specifically, regions of validity are established for each approximation by comparing exact Mie value against the corresponding approximate value. A wide range of size parameters and indices of refraction were considered in the analysis. In addition, the regions of validity are represented in a way that that permits the various approximations to be intercompared. The purpose of this latter test is to see where better approximations are needed.

4.1 Approximations That Were Investigated

Five approximations for Q_{ext} have been investigated in this report: two for small particles[6,7] and three for large particles[4,8,9]. For Q_{abs}, a total of seven approximations were looked at: those given by [4,6-9], plus two other approximations for large particles[10,11]. A brief description of

---

6. Rayleigh, Lord (1871) On the light from the sky, its polarization and colour, Philos. Mag., 41:107-120, 274-279 (reprinted in Scientific Papers by Lord Rayleigh, Vol. I:1869-1881, No. 8, Dover, New York, 1964).
7. Wiscombe, W. (1980) Improved Mie scattering algorithms, Appl. Opt., 9:1505-1509.
8. Deirmendjian, D. (1969) Electromagnetic Scattering on Spherical Polydispersions, Elsevier, New York.
9. Ackerman, S. A. and Stephens, G. L. (1987) The absorption of solar radiation by cloud droplets: an application of anomalous diffraction theory, J. Atmos. Sci., 44:1574-1588.
10. Bohren, C. F. and Nevitt, T. (1983) Absorption by a sphere: A simple approximation, Appl.Opt., 22:774-775.

how each approximation works is given in Table 3. For reference, the equations governing the various approximations have been reproduced in Appendix A of this report.

4.2 Comparison Scheme

4.2.1 Realm of Comparison

Table 4 summarizes the size parameters and complex indices of refraction that are investigated in the current analysis. These values encompass the realm of particles normally encountered in atmospheric aerosol modeling. For each approximation, n is held fixed and the exact Mie and approximate values are calculated at incremental steps of the size parameter, X, and the imaginary index of refraction, k. The steps are equally spaced in the logarithms of X and k where the spacing consists of fifty steps per decade of X and twenty five steps per decade of k. Similar sets of data are also computed for other fixed values of n.

4.2.2 Smoothing Function

Before constructing error plots, data for Mie theory and the approximations have been convolved with an eleven point smoothing function, S. Specifically, the smoothing function is passed over the data for $X \geq 1$ while k is held

---

11. Levine, P. H. (1978) Absorption efficiency for large spherical particles: A new approximation, Appl. Opt., 17:3861-3862.

Table 3. Summary of the Approximations That Were Investigated

RESEARCHER	PARTICLE SIZE	Q_{ext}	Q_{abs}	BRIEF DESCRIPTION
Rayleigh[6]	Small	Yes	Yes	Radiation emitted by an oscillating dipole
Wiscombe[7]	Small	Yes	Yes	Retention of first-order terms in the Mie expansion
Deirmendjian[8]	Large	Yes	Yes	Applies an empirical correction to the anomalous diffraction theory of van de Hulst[1]
Ackerman and Stephens[9]	Large	Yes	Yes	Uses the anomalous diffraction theory of van de Hulst[1] plus first order corrections for refraction and edge effects
Nussenzveig and Wiscombe[4]	Large	Yes	Yes	Complex angular momentum theory
Bohren and Nevitt[10]	Large	No	Yes	Expression is developed from the laws governing geometrical optics
Levine[11]	Large	No	Yes	Uses the van de Hulst[1] expression in the large particle limit plus a correction term for front surface reflections

Table 4. Particle Characteristics That Were Investigated

PARAMETER	RANGE
Real Part of the Index of Refraction, n	1.1 - 3.0
Imaginary Part of the Index of Refraction, k	10^{-6} - 10
Size Parameter, X	10^{-2} - 10^{3}

fixed so that

$$\bar{F}_{X_i} = \sum_{L=0}^{10} S_L F_{X_{i+L-5}} \tag{22}$$

where F_{X_i} represents the Mie or approximate value at consecutive steps of the size parameter, X_i. The weighting factors for the smoothing function are given by

$$S_L = \frac{\binom{10}{L}}{1024} \quad , \; L = 0, 1, \ldots, 10 \tag{23}$$

where $\binom{10}{L}$ is the binomial coefficient,

$$\binom{10}{L} = 10!/((L!)(10-L)!) \; . \tag{24}$$

The smoothing function acts to eliminate the high-frequency ripple structure that occurs in the exact Mie values

for the efficiency factors as a function of X for fixed k. For reference, the ripple structure in Q_{sct} is illustrated in Figure 11 for fixed values of k. The reason for eliminating the ripple structure is twofold:

1) it allows for a fairer assessment of the various approximations because the ripple structure can only be calculated with Mie theory

2) since many aerosol modeling applications involve a polydispersion of particles, the effects of the ripples are "washed out" when integrating over particle size.

The width of the smoothing function has been chosen to preserve the large scale oscillations, known as interference structure.

4.2.3 Percent Error Contour Plots

For each approximation, two-dimensional percent error diagrams have been developed for fixed values of n. The percent errors are computed by

$$E_{X_i,k_j} = 100(A_{X_i,k_j} - M_{X_i,k_j})/M_{X_i,k_j} \qquad (25)$$

where A and M are the (smoothed) approximate and Mie values, respectively, evaluated at size parameter X_i and imaginary index of refraction k_j. Contour lines have been drawn for percent errors of 8, 20 and 50%.

4.3 Results

4.3.1 Regions of Validity for the Extinction Approximations

Figures 12(a) - 12(e) give representative percent error diagrams for each of the extinction approximations. Each plot is for n = 1.54, and the regions where percent errors

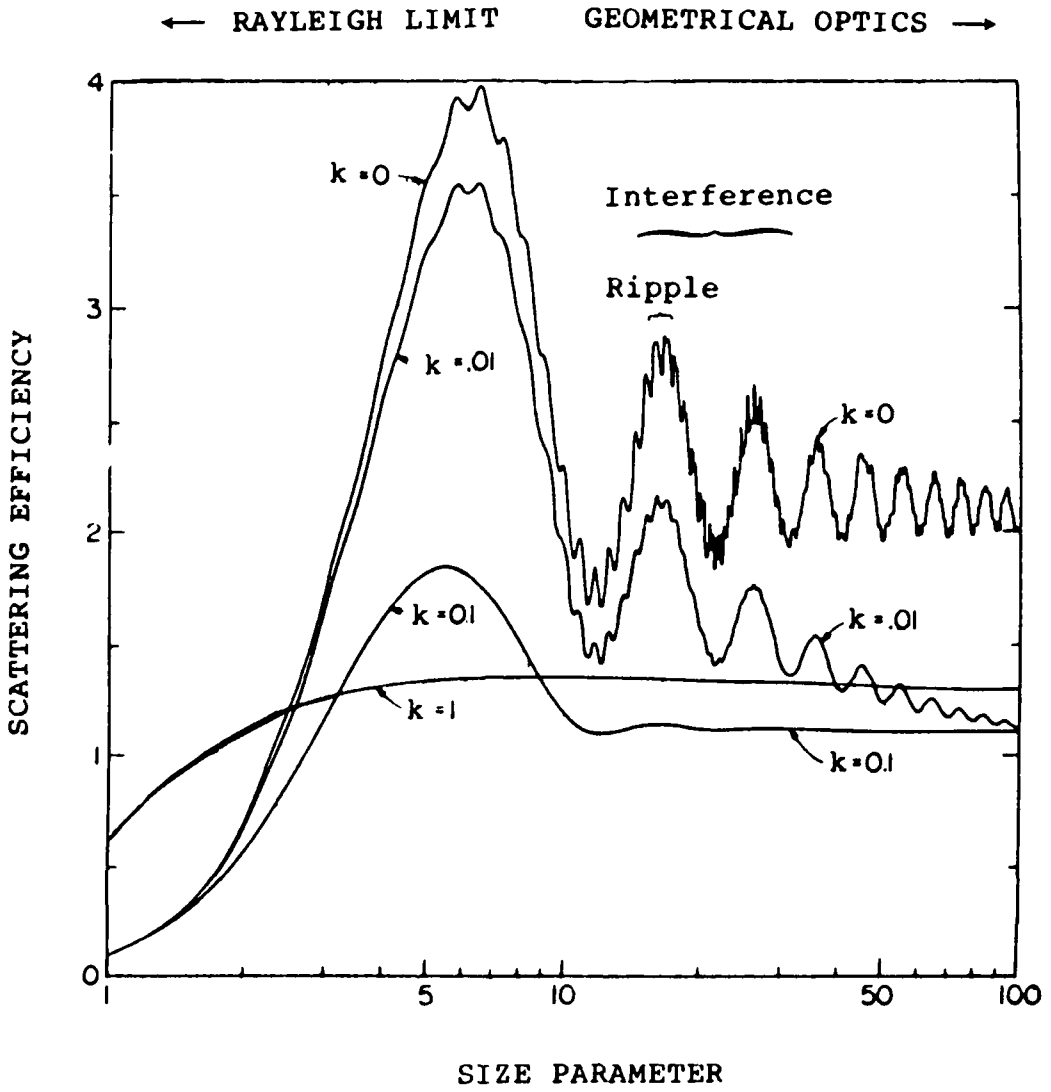

Figure 11. Mie Theory Calculations of Q_{sct} Showing the Interference and Ripple Structure as a Function of Size Parameter and k for Fixed n (= 1.33)

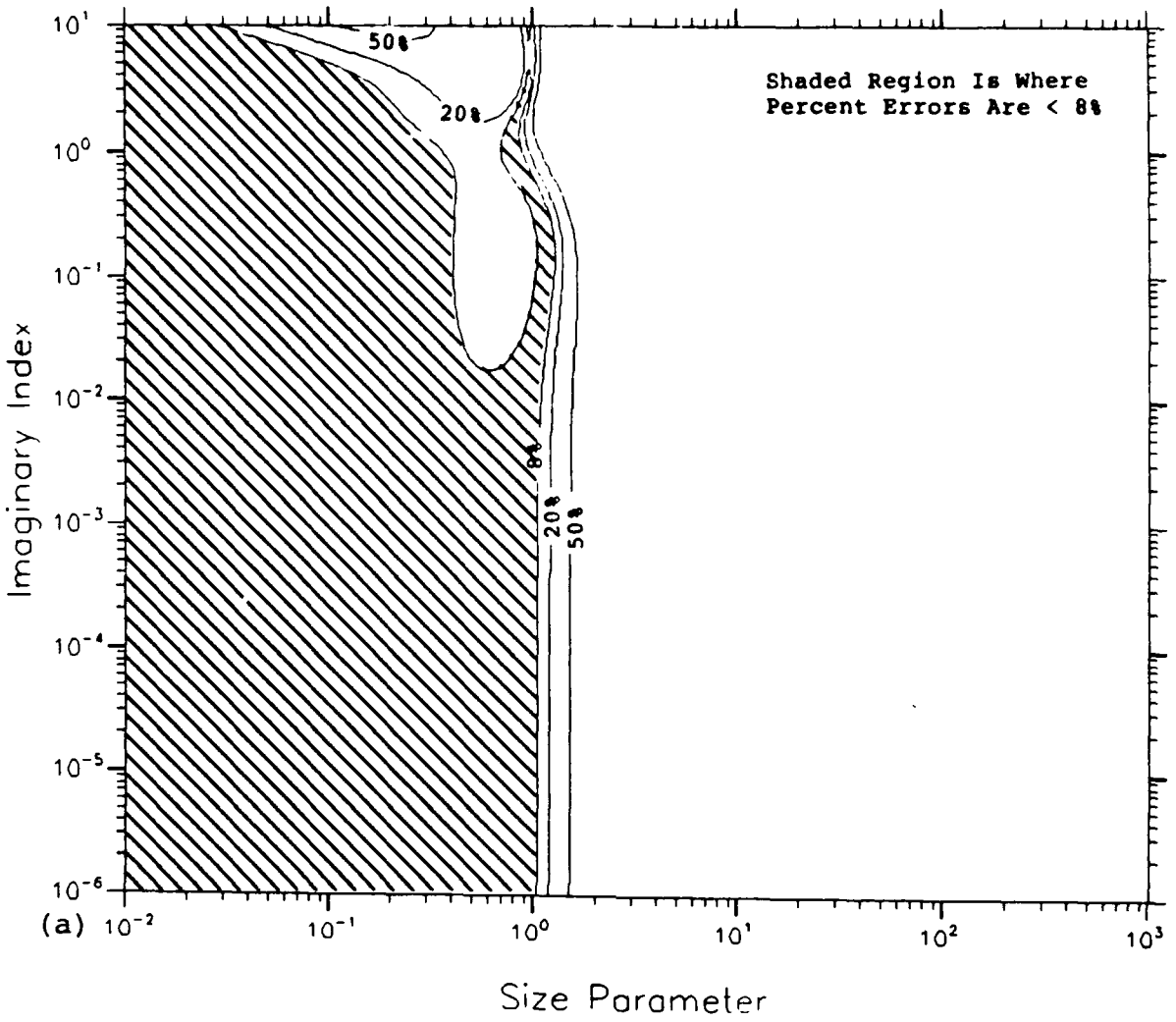

Figure 12. Percent Errors in Q_{ext} for the Approximation of (a) Rayleigh, for n = 1.54

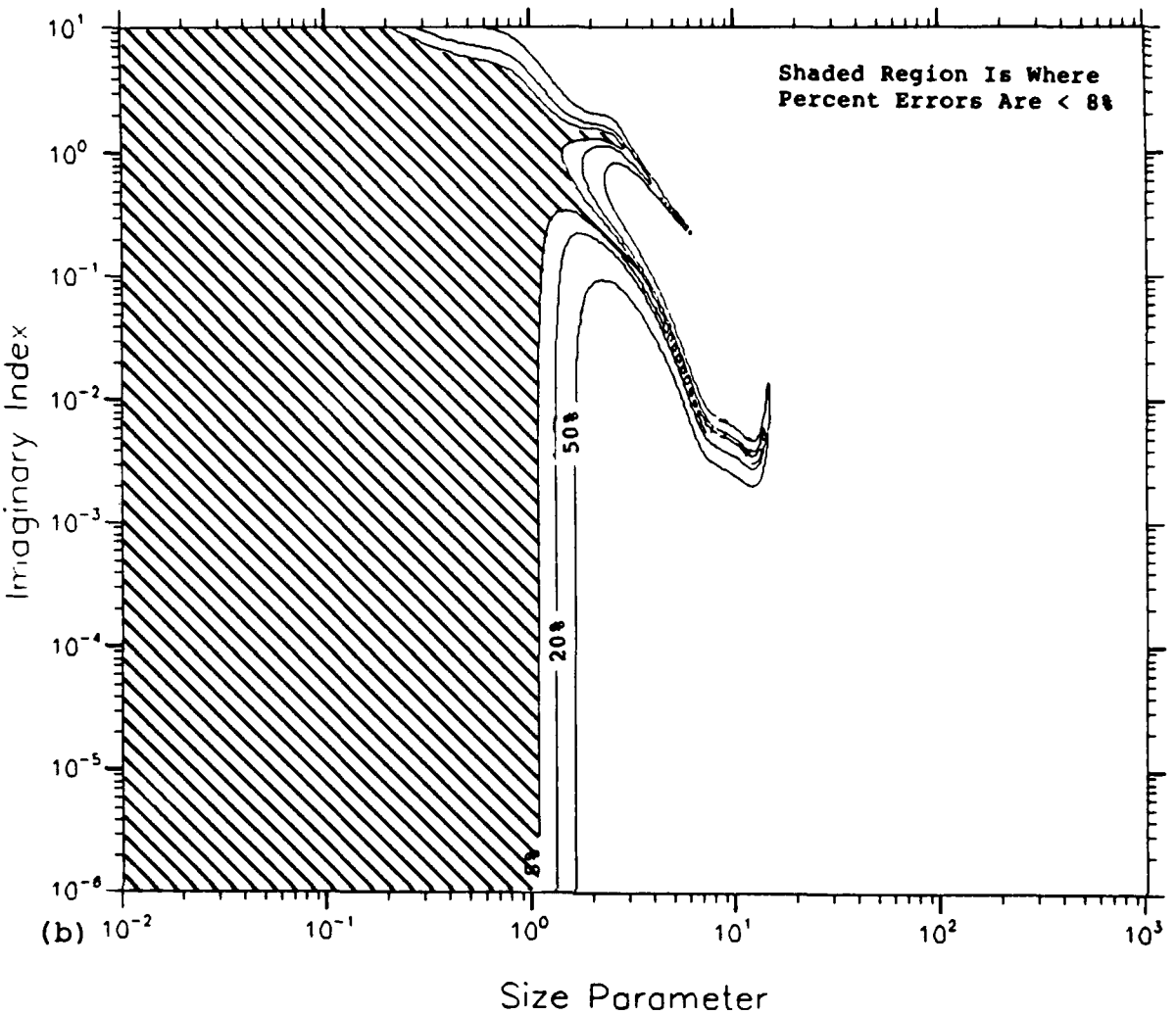

Figure 12. (continued) Percent Errors in Q_{ext} for the Approximation of (b) Wiscombe, for n = 1.54

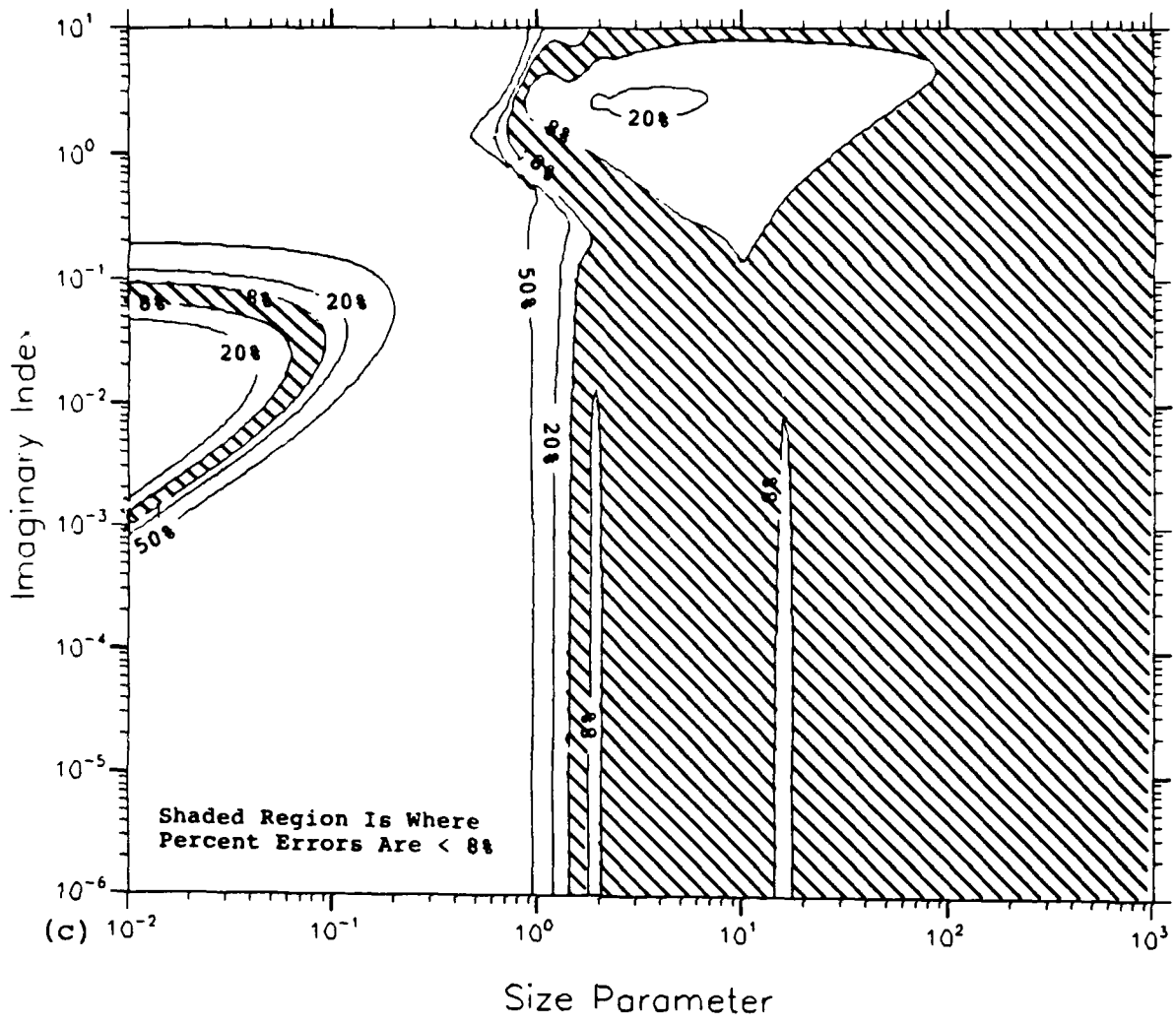

Figure 12. (continued) Percent Errors in Q_{ext} for the Approximation of (c) Deirmendjian, for n = 1.54

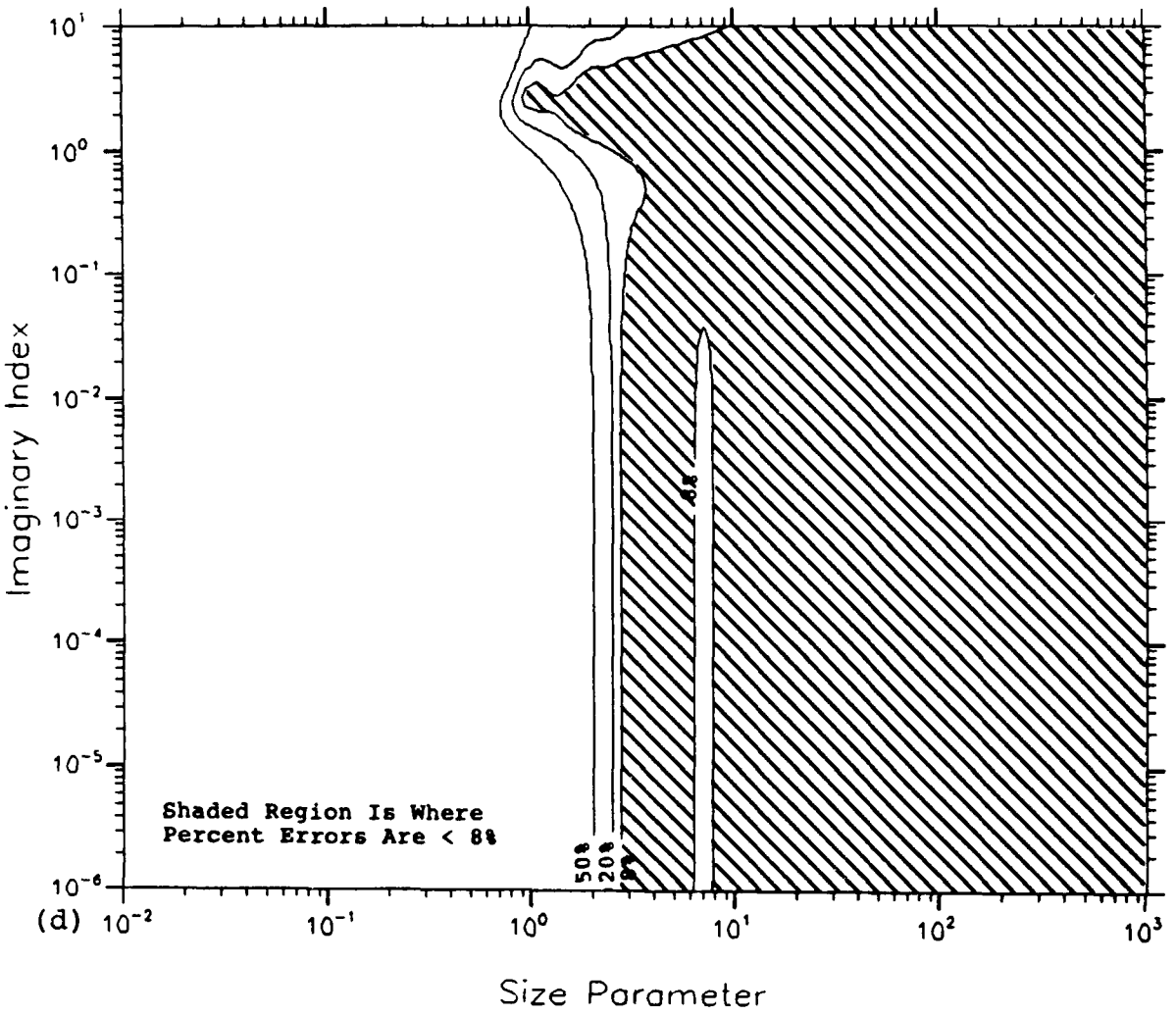

Figure 12. (continued) Percent Errors in Q_{ext} for the Approximation of (d) Ackerman and Stephens, for n = 1.54

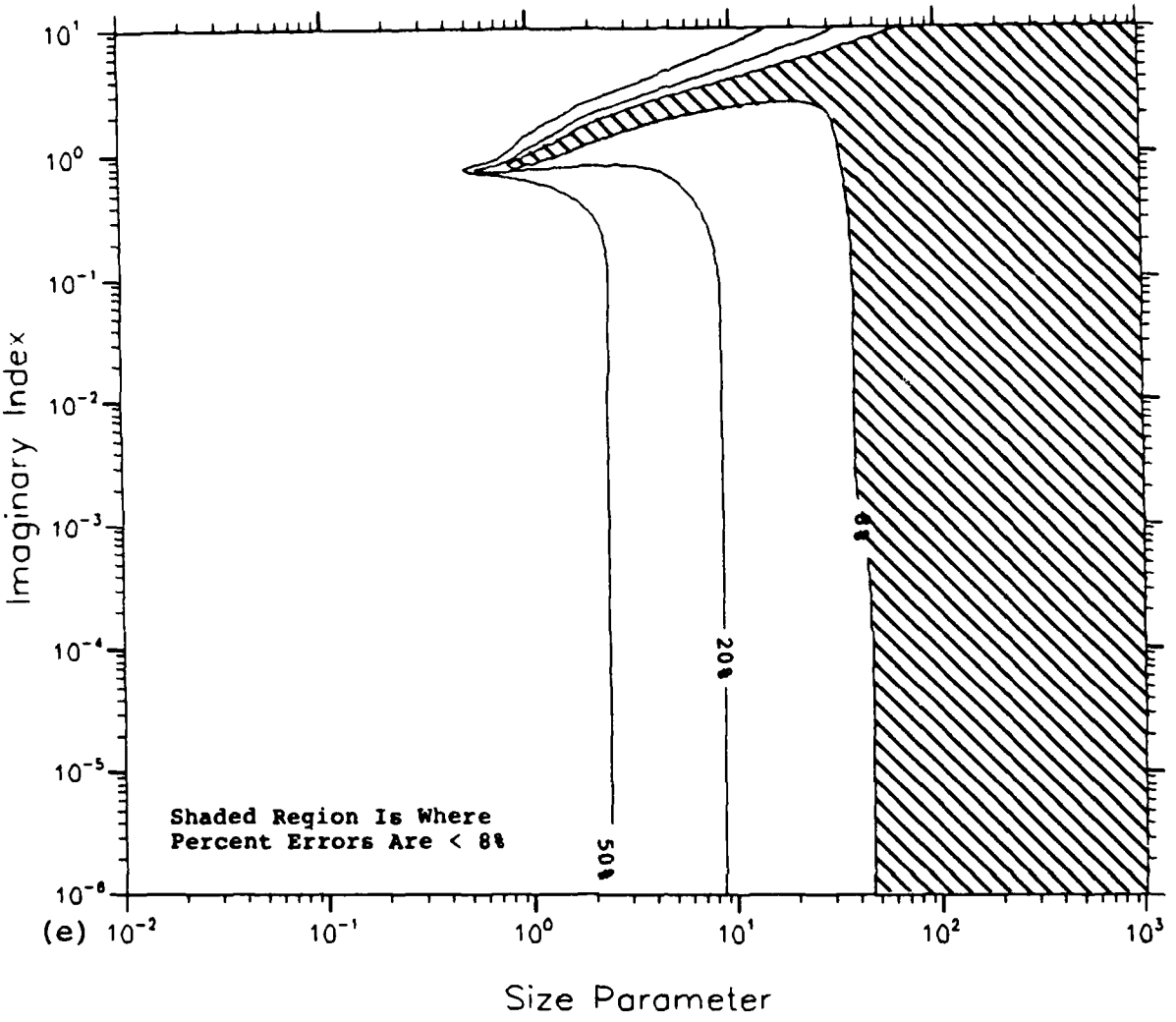

Figure 12. (continued) Percent Errors in Q_{ext} for the Approximation of (e) Nussenzveig and Wiscombe, for n = 1.54

are less than 8% have been shaded. For brevity, plots for other values of n have not been included here.

Figures 12(a) - 12(e), and similar plots for other n, have been used to determine the regions of validity of the various approximations for Q_{ext}. These results are given in Figure 13. The dashed line for the Nussenzveig and Wiscombe approximation indicates the useful range if the singularity that arises for odd integer values of n is avoided (see Section 3.4).

In general, existing approximations for Q_{ext} do reasonably well for both large and small size parameters. Of the large particle approximations, the Ackerman and Stephens approximation extends to the lowest size parameter. If higher accuracies are needed (i.e. 0.1 to 1% or better), the Nussenzveig and Wiscombe approximation has a wider useful range than the other large particle approximations because it reproduces the higher-order ripple structure better. Most approximations however, have trouble predicting the magnitude and location of the first interference peak which occurs between size parameters of 1 and 10 (see Figure 11). On the other hand, percent errors within this narrow band are generally less than 20% for many of the approximations.

4.3.2 Regions of Validity for the Absorption Approximations

Figures 14(a) - 14(g) give representative percent error diagrams for each of the absorption approximations. Each plot is for n = 1.54, and the regions where percent errors

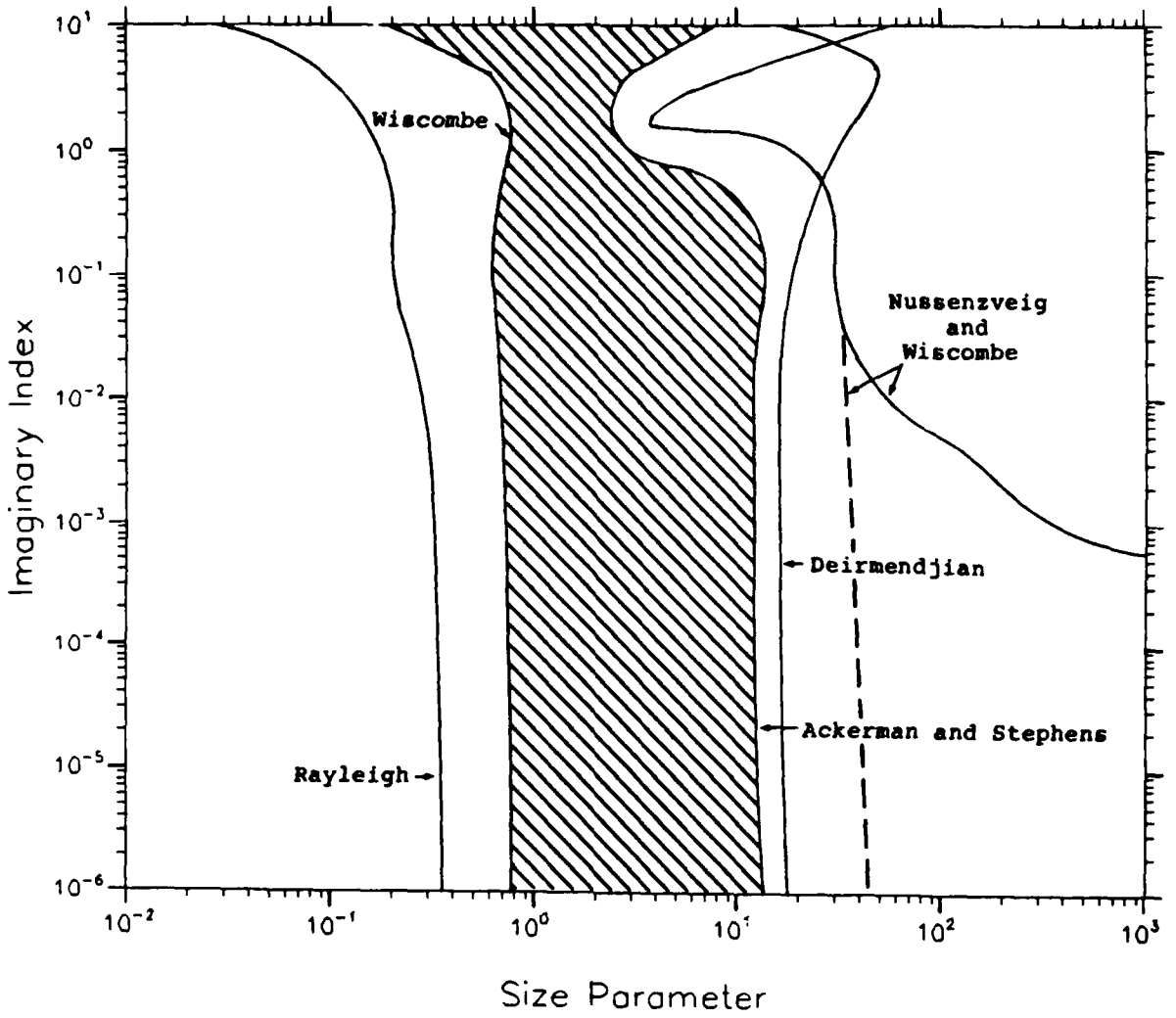

Figure 13. Regions of Validity for the Mie Approximations for Q_{ext}. The Shaded Regions Indicates Where All of the Approximations Give Percent Errors > 8%. The Dashed Line for the Nussenzveig and Wiscombe Approximation Indicates the Useful Range If the Singularity That Arises for Odd Integer Values of n Is Avoided

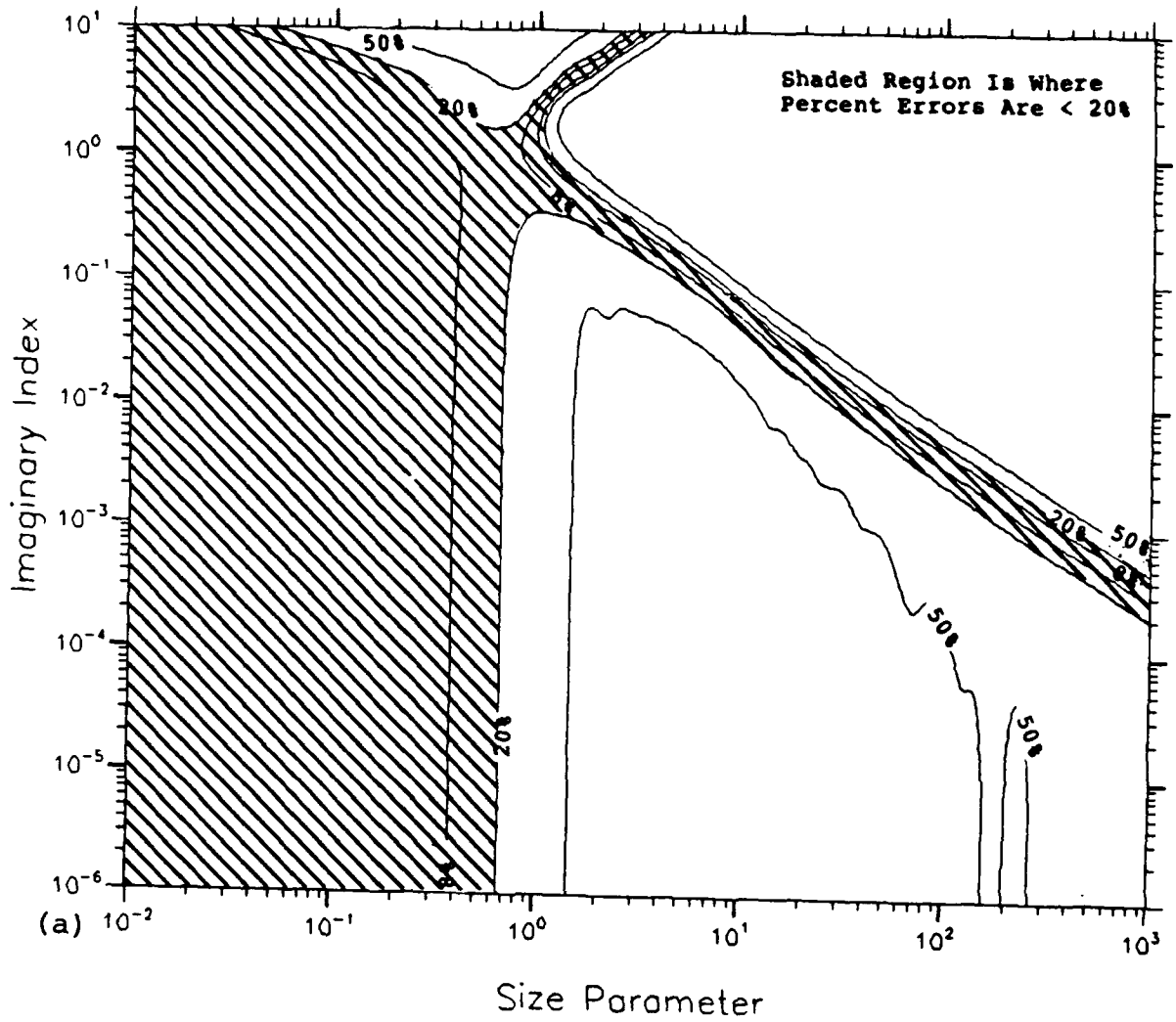

Figure 14. Percent Errors in Q_{abs} for the Approximation of (a) Rayleigh, for n = 1.54

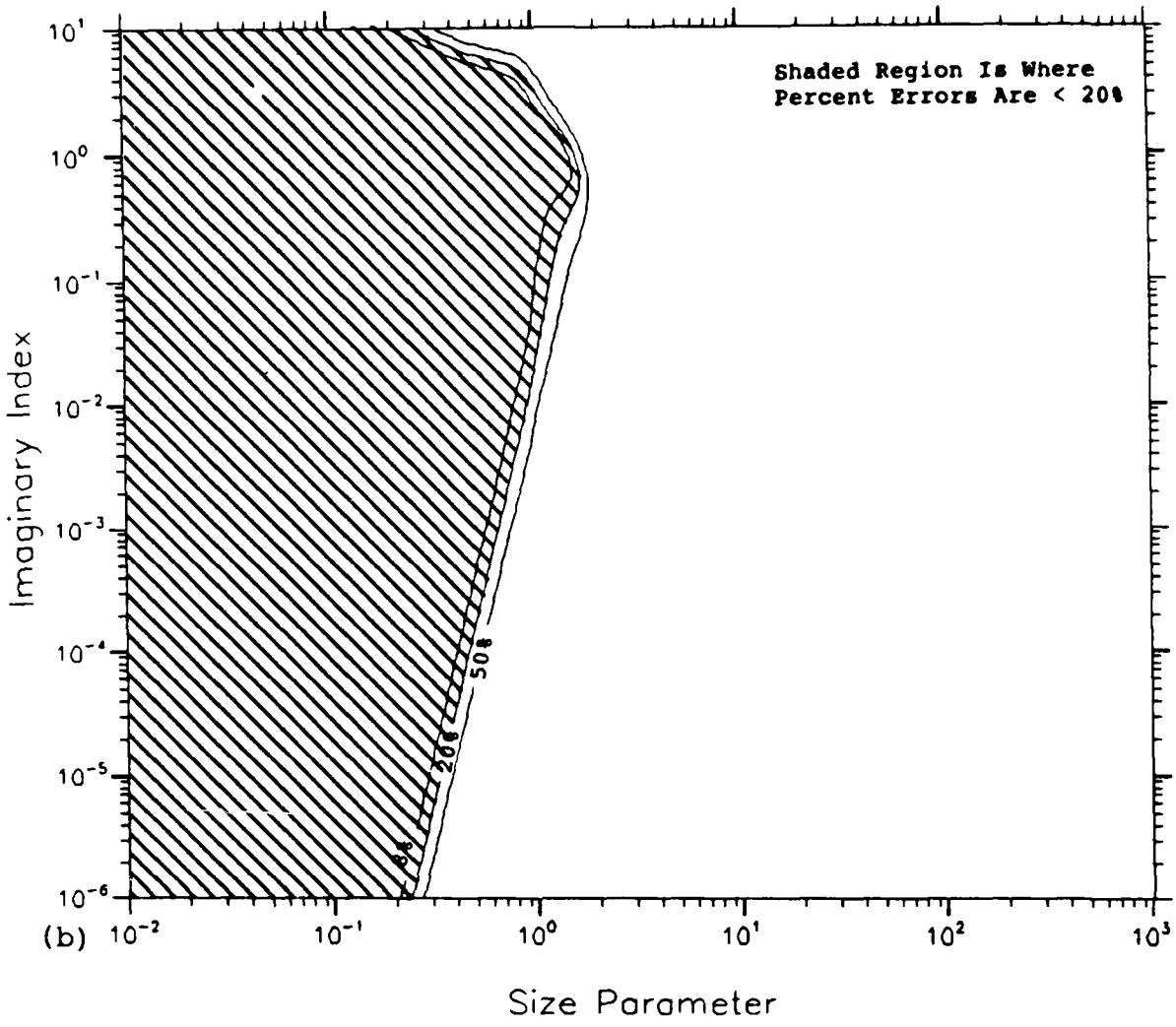

Figure 14. (continued) Percent Errors in Q_{abs} for the Approximation of (b) Wiscombe, for n = 1.54

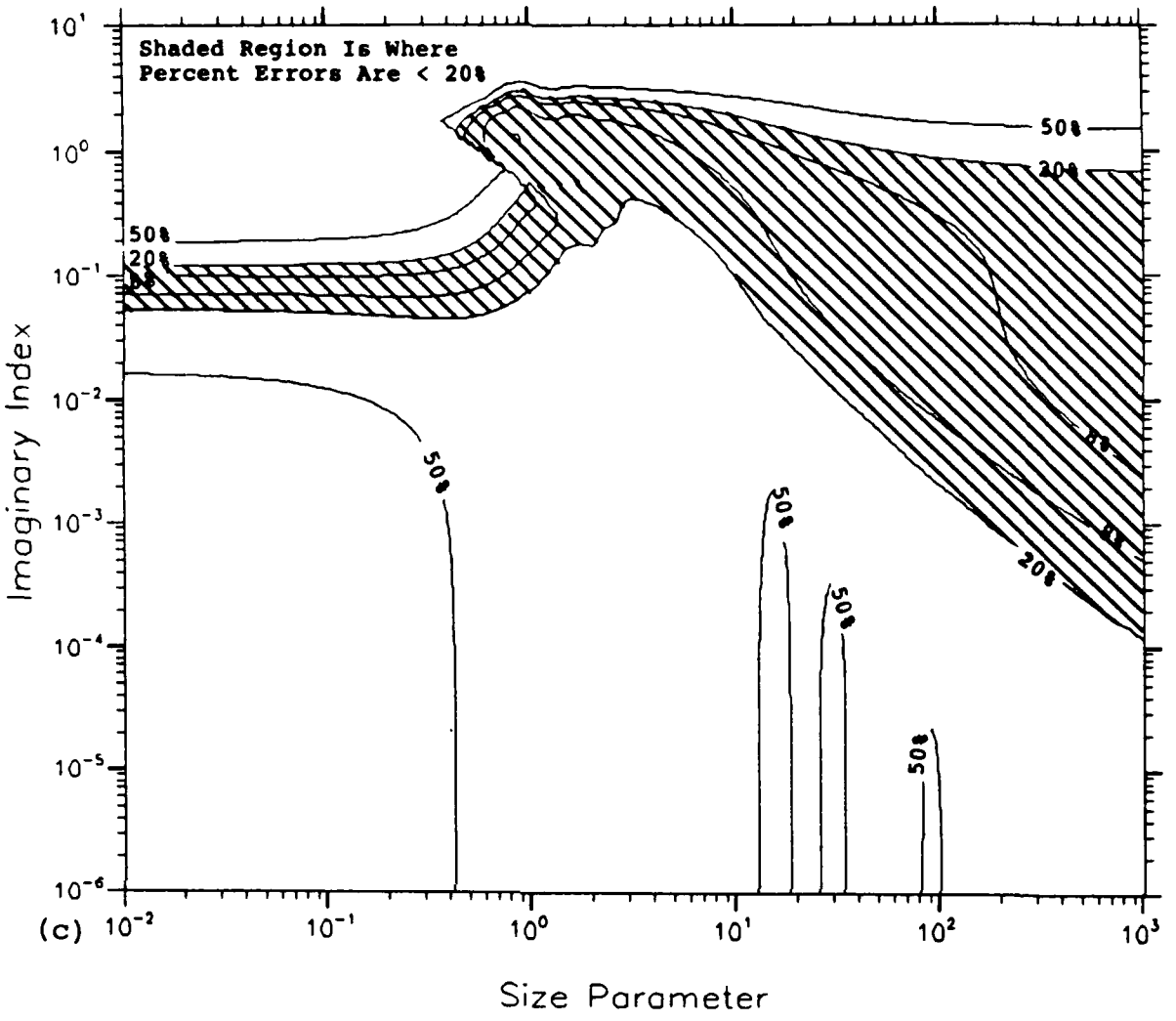

Figure 14. (continued) Percent Errors in Q_{abs} for the Approximation of (c) Deirmendjian, for n = 1.54

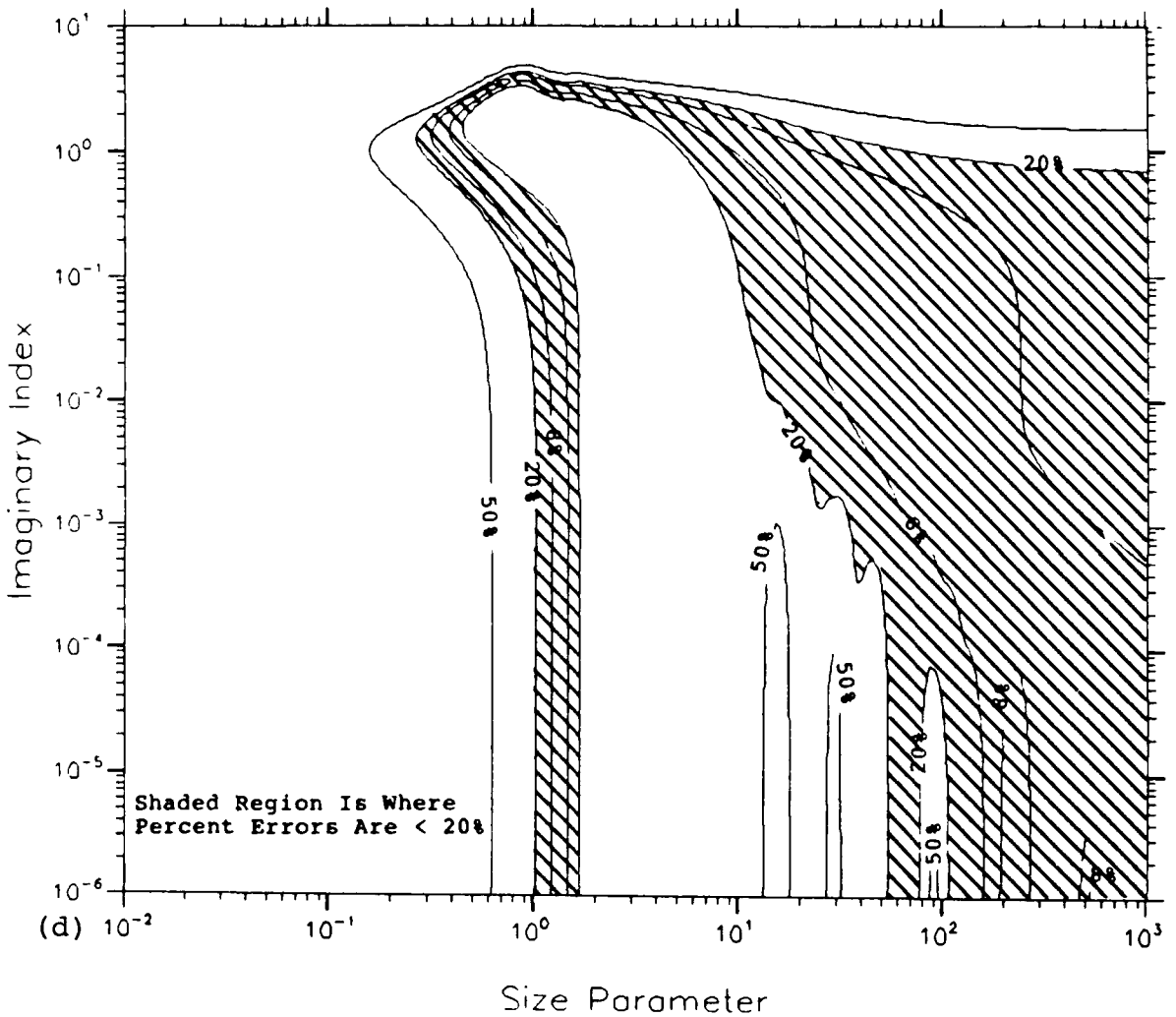

Figure 14. (continued) Percent Errors in Q_{abs} for the Approximation of (d) Ackerman and Stephens, for n = 1.54

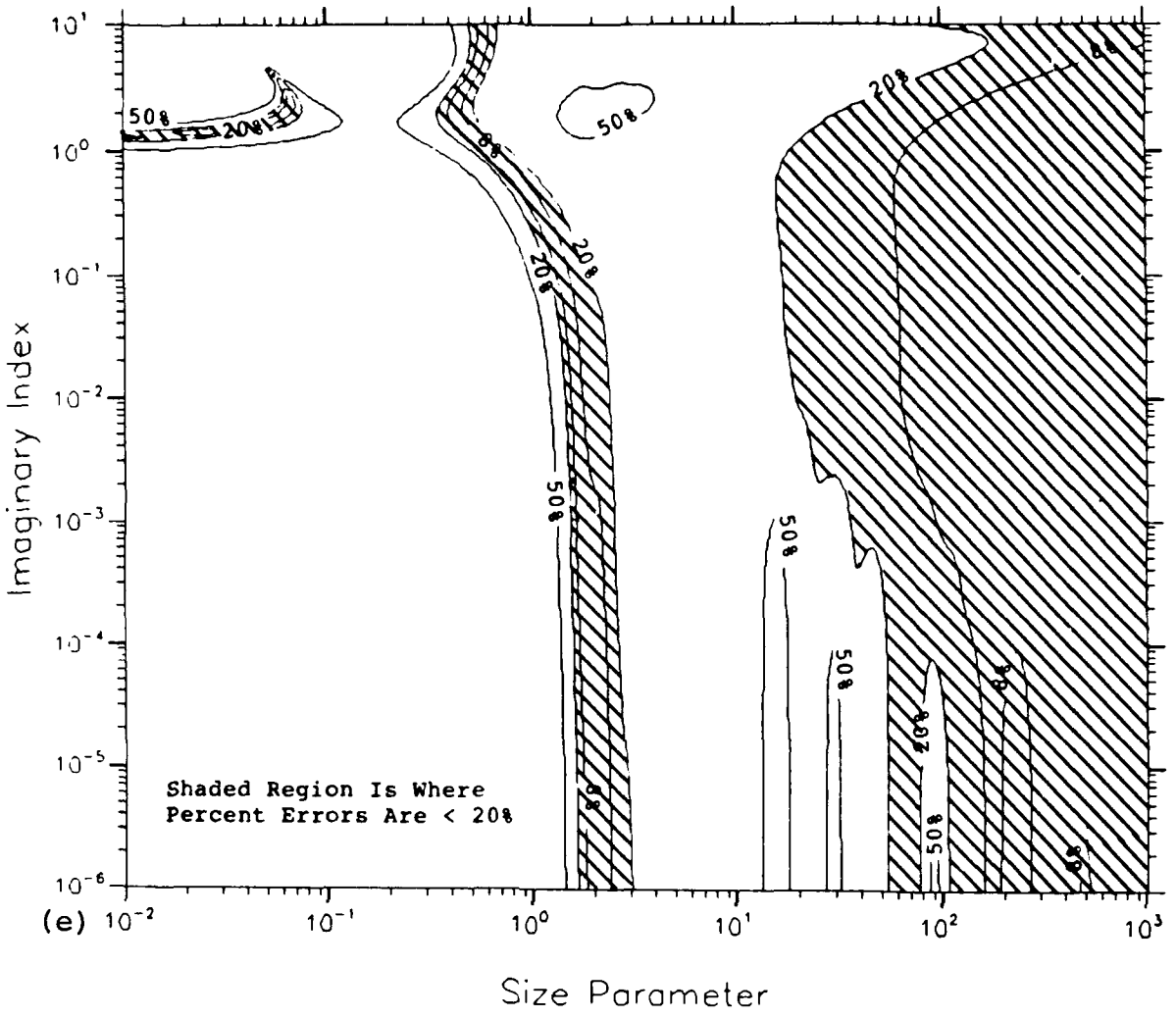

Figure 14. (continued) Percent Errors in Q_{abs} for the Approximation of (e) Nussenzveig and Wiscombe, for n = 1.54

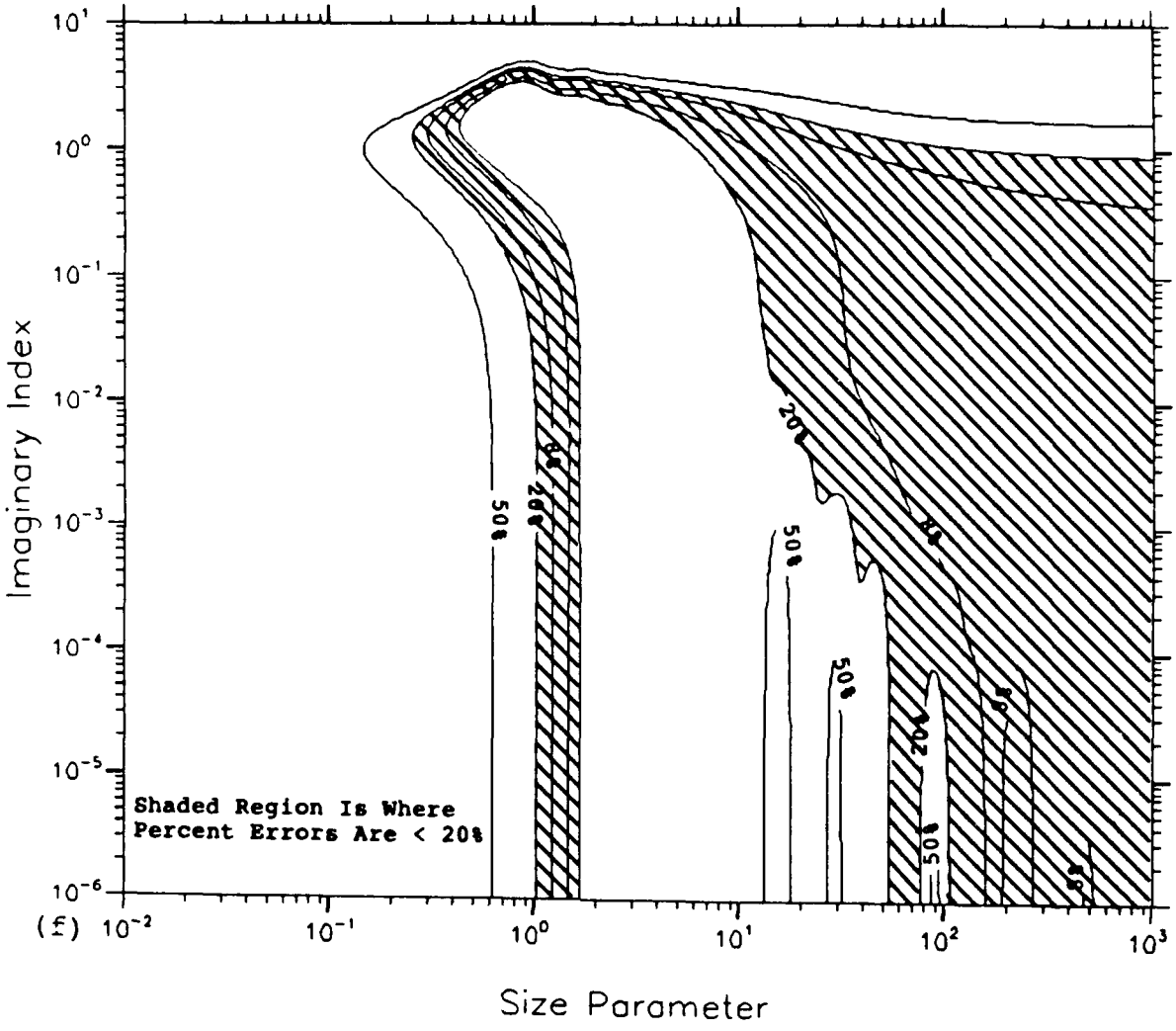

Figure 14. (continued) Percent Errors in Q_{abs} for the Approximation of (f) Bohren and Nevitt, for $\tilde{n} \cong 1.54$

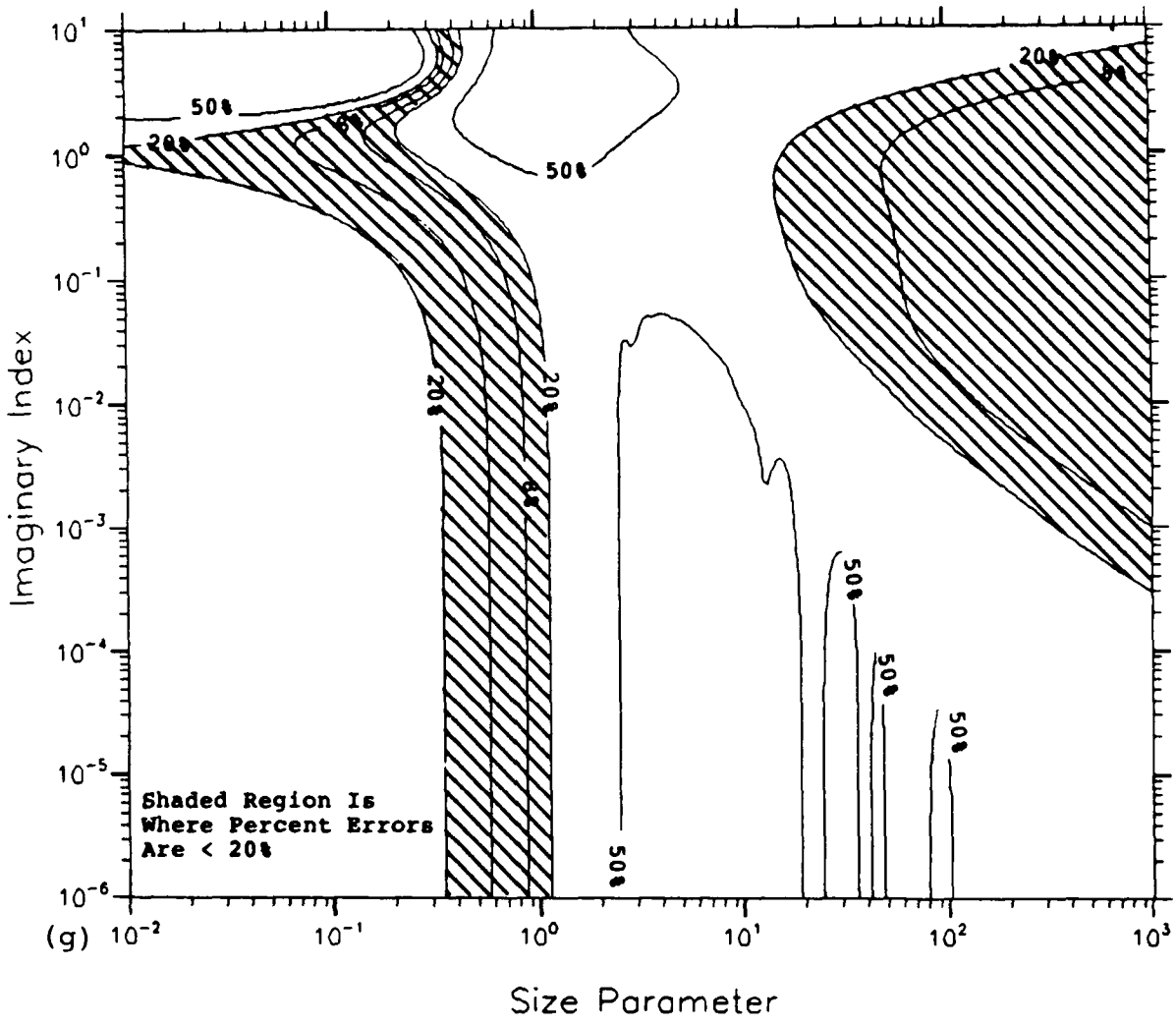

Figure 14. (continued) Percent Errors in Q_{abs} for the Approximation of (g) Levine, for n = 1.54

are less than 20% have been shaded. For brevity, plots for other n have not been included here.

Figures 14(a) - 14(g), and similar plots for other n, have been used to determine the regions of validity of the various approximations for Q_{abs}. These results are given in Figure 15. The region of validity of the Nussenzveig and Wiscombe approximation is drawn with a dashed line because it is only computionally efficient for size parameters greater than about 200, relative to exact Mie theory (see Section 3.3), where it is accurate to about 0.1%. Also, to avoid clutter, the region of validity of the Ackerman and Stephens approximation has not been shown; however, its omission does not alter the shape of the shaded region in Figure 15 because the Ackerman and Stephens approximation for Q_{abs} is similar to the Bohren and Nevitt approximation.

Figure 15 suggests that existing approximations for Q_{abs} are less accurate than those for Q_{ext}. For example, the tolerable error has been relaxed to 20% because significant errors extend to rather large size parameters. Of the large particle approximations, the Bohren and Nevitt approximation appears to have the largest region of applicability. In contrast to Figure 13, the percent errors within the shaded region of Figure 15 often exceed 50%.

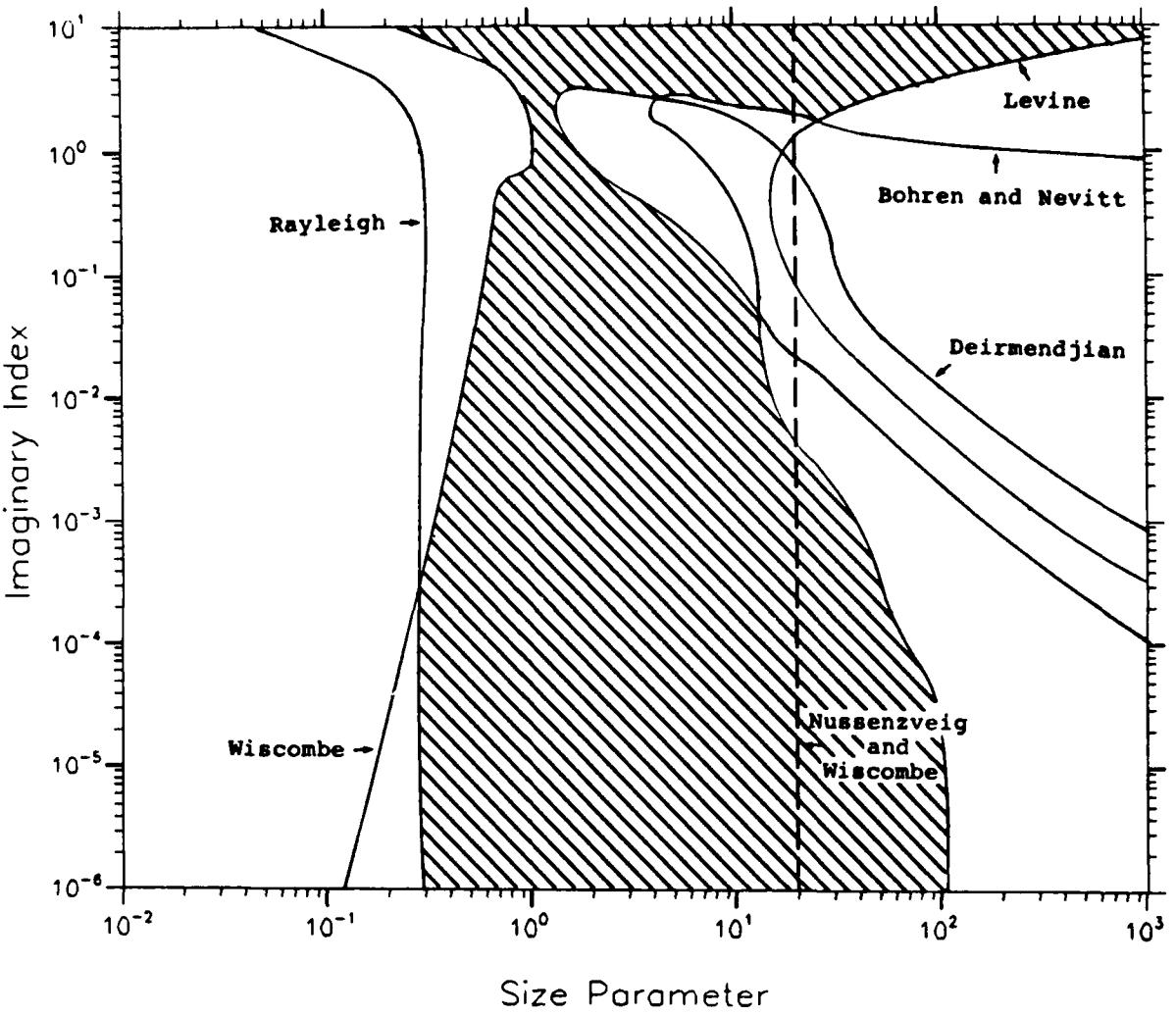

Figure 15. Regions of Validity for the Mie Approximations for Q_{abs}. The Shaded Regions Indicates Where All of the Approximations Give Percent Errors > 20%. The Ackerman and Stephens Approximation Is Omitted for Clarity, But Is Similar to That of Bohren and Nevitt. The Nussenzveig and Wiscombe Approximation Is Shown with a Dashed Line Because It Is Only Computationally Efficient for X > 200

5. SUMMARY AND CONCLUSIONS

This report has explored alternative algorithms to Mie theory. Specifically, Chapter 2 discussed the use of ray optics to calculate the phase matrix elements of polydisperse spheres in geometrical optics limit. Generally speaking, ray optics should be used for size parameters greater than 400, and becomes more accurate for particles containing significant absorption. Chapter 3 explored the use of complex angular momentum theory to determine Q_{ext}, Q_{abs} and Q_{pr} (or g). It was shown that although accurate for size parameters greater than 20, this technique is only computationally efficient for size parameters greater than 500. In Chapter 4, approximations for Q_{ext} and Q_{abs} in the scientific literature were investigated and their regions of validity were established. It was shown that existing approximations can give reasonable estimates of Q_{ext} for most size parameters and complex indices of refraction. On the other hand, the approximations for Q_{abs} are much less accurate.

References

1. van de Hulst, H. C. (1957) Light Scattering by Small Particles, Wiley, Inc., New York, 470 pp.

2. Liou, K., and Hansen, J. E. (1971) Intensity and polarization for single scattering by polydisperse spheres: A comparison of ray optics and Mie theory, J. Atmos. Sci. 28:995-1004.

3. Blattner, W. (1972) Utilization instructions for operation of the Mie programs on the CDC-6600 computer at AFCRL, F19628-70-C-0156, Research Note, RRA-N7240, Radiation Research Associates, Inc., Fort Worth, Texas.

4. Nussenzveig, H. M., and Wiscombe, W. J. (1980) Effi ciency factors in Mie scattering, Phys. Rev Letters., 45:1490-1494.

5. Wiscombe, W. J., private communication.

6. Rayleigh, Lord (1871) On the light from the sky, its polarization and colour, Philos. Mag., 41:107-120, 274-279 (reprinted in Scientific Papers by Lord Rayleigh, Vol. I:1869-1881, No. 8, Dover, New York, 1964).

7. Wiscombe, W. (1980) Improved Mie scattering algorithms, Appl. Opt., 9:1505-1509.

8. Deirmendjian, D. (1969) Electromagnetic Scattering on Spherical Polydispersions, Elsevier, New York.

9. Ackerman, S. A. and Stephens, G. L. (1987) The absorption of solar radiation by cloud droplets: an application of anomalous diffraction theory, J. Atmos. Sci., 44:1574-1588.

10. Bohren, C. F. and Nevitt, T. (1983) Absorption by a sphere: A simple approximation, Appl.Opt., 22:774-775.

11. Levine, P. H. (1978) Absorption efficiency for large spherical particles: A new approximation, Appl. Opt., 17:3861-3862.

Appendix A

Equations for the Various Mie Approximations Investigated in this Report

This appendix gives the equations used to calculate the extinction efficiency, Q_{ext}, and the absorption efficiency, Q_{abs}, for the Mie approximations discussed in this report. For some of the approximations, the scattering efficiency, Q_{sca}, is calculated in place of either Q_{ext} or Q_{abs} where the three terms are then related by $Q_{ext} = Q_{sca} + Q_{abs}$. The list of equations serves only as an overview and the reader should consult the original references for more detailed information. Also, some of notation from the original references has been changed such that it is consistent with the terminology used in this report. In the equations below, X represents the particle size parameter and $m = n + ik$ represents the complex index of refraction of the particle.

Equations for the Rayleigh Approximation[6]

The Rayleigh approximation for Q_{abs} is computed as

$$Q_{abs} = 4X \, \mathrm{Im}\left\{\frac{m^2 - 1}{m^2 + 2}\right\} \qquad \text{(A-1)}$$

and Q_{sca} is given by

$$Q_{sca} = \frac{8}{3} X^4 \left|\frac{m^2 - 1}{m^2 + 2}\right|^2 \qquad \text{(A-2)}$$

where $Q_{ext} = Q_{sca} + Q_{abs}$.

Equations for the Wiscombe Approximation[7]

The Wiscombe approximation for Q_{ext} is computed as

$$Q_{ext} = 6X\,\mathrm{Re}\left(\hat{a}_1 + \hat{b}_1 + \frac{5}{3}\hat{a}_2\right) \qquad \text{(A-3)}$$

and Q_{sca} is given by

$$Q_{sca} = 6X^4 T \qquad \text{(A-4)}$$

where $Q_{abs} = Q_{ext} - Q_{sca}$ and

$$\hat{a}_1 = 2i\frac{m^2-1}{3}\frac{1-\frac{1}{10}X^2+\frac{4m^2+5}{1400}X^4}{D} \qquad \text{(A-5)}$$

$$\hat{b}_1 = iX^2\frac{m^2-1}{45}\frac{1+\frac{2m^2-5}{70}X^2}{1-\frac{2m^2-5}{30}X^2} \qquad \text{(A-6)}$$

$$\hat{a}_2 = iX^2\frac{m^2-1}{15}\frac{1-\frac{1}{14}X^2}{2m^2+3-\frac{2m^2-7}{14}X^2} \qquad \text{(A-7)}$$

$$D = m^2+2+\left(1-\frac{7}{10}m^2\right)X^2-\frac{8m^4-385m^2+350}{1400}X^4 + 2i\frac{m^2-1}{3}X^3\left(1-\frac{1}{10}X^2\right) \qquad \text{(A-8)}$$

and

$$T = \left|\hat{a}_1\right|^2+\left|\hat{b}_1\right|^2+\frac{5}{3}\left|\hat{a}_2\right|^2 \qquad \text{(A-9)}$$

Equations for the Deirmendjian Approximation[8]

The Deirmendjian approximation for Q_{ext} is computed as

$$Q_{ext} = Q_{VHext}(1 + D) \tag{A-10}$$

and Q_{abs} is given by

$$Q_{abs} = Q_{VHabs}(1 + D) \tag{A-11}$$

where Q_{VHext} is the extinction efficiency from van de Hulst[1],

$$Q_{VHext} = 2 - \frac{4\cos\beta}{\rho}\exp(-\rho\tan\beta)\sin(\rho-\beta)$$

$$+ 4\left(\frac{\cos\beta}{\rho}\right)^2[\cos 2\beta - \exp(-\rho\tan\beta)\cos(\rho - 2\beta)] \tag{A-12}$$

and Q_{VHabs} is the absorption efficiency from van de Hulst[1],

$$Q_{VHabs} = 1 + \frac{\exp(-2\rho\tan\beta)}{\rho\tan\beta} + \frac{\exp(-2\rho\tan\beta) - 1}{2(\rho\tan\beta)^2} \tag{A-13}$$

where

$$\beta = \tan^{-1}\left(\frac{k}{n-1}\right) \tag{A-14}$$

and

$$\rho = 2X(n-1) \tag{A-15}$$

In Eqs. A-10 and A-11, the correction term, D, is given by

$$D = \begin{cases} \dfrac{(n-1)^2}{1.632n}[f(\beta)+1] + \dfrac{0.2\rho - n + 1}{(n-1)f(\beta)} & \text{for } \rho \le 5(n-1) \\ \dfrac{n-1}{8.16n}[f(\beta)+1]\rho & \text{for } 5(n-1) \le \rho \le \dfrac{4.08}{1+3\tan\beta} \\ \dfrac{(n-1)[f(\beta)+1]}{2n(1+3\tan\beta)} & \text{for } \dfrac{4.08}{1+3\tan\beta} \le \rho \le \dfrac{4.08}{1+\tan\beta} \\ \dfrac{2.04(n-1)[f(\beta)+1]}{nf(\beta)\rho} & \text{for } \rho > \dfrac{4.08}{1+\tan\beta} \end{cases} \qquad \text{(A-16)}$$

where

$$f(\beta) = 1 + 4\tan\beta + 3\tan^2\beta \quad . \qquad \text{(A-17)}$$

Equations for the Ackerman and Stephens Approximation[9]

The Ackerman and Stephens approximation for Q_{ext} is computed as

$$Q_{ext} = 2 - \frac{4m^2}{\rho} e^{-\rho \tan\beta} \left[\cos\beta \sin(\rho - \beta) + \frac{\cos^2\beta}{\rho} \cos(\rho - 2\beta) \right]$$

$$+ \frac{4m^2}{\rho} e^{-\rho \tan\beta \sqrt{1 - m^{-2}}} \left[\sqrt{1 - m^{-2}} \cos\beta \right.$$

$$\left. \times \sin\left(\rho\sqrt{1 - m^{-2}} - \beta\right) + \frac{\cos^2\beta}{\rho} \cos\left(\rho\sqrt{1 - m^{-2}} - 2\beta\right) \right] \quad \text{(A-18)}$$

and Q_{abs} is given by

$$Q_{abs} = 2 + \frac{m^2}{2Xk} e^{-4Xk} \left[1 + (4Xk)^{-1} \right]$$

$$- \frac{m}{2Xk} e^{-4Xk\sqrt{1 - m^{-2}}} \left(\sqrt{m^2 - 1} + \frac{m}{4Xk} \right) \quad \text{(A-19)}$$

where

$$\beta = \tan^{-1}\left(\frac{k}{n - 1}\right) \quad \text{(A-20)}$$

and

$$\rho = 2X(n - 1) \quad \text{(A-21)}$$

Equations for the Nussenzveig and Wiscombe Approximation[4]

The Nussenzveig and Wiscombe approximation for Q_{ext} is computed as

$$Q_{ext} = 2 + 1.9923861\,X^{-\frac{2}{3}} + 8\,\mathrm{Im}\left\{\tfrac{1}{4}(m^2+1)(m^2-1)^{-\frac{1}{2}}X^{-1}\right.$$

$$- m^2(m+1)^{-1}(m^2-1)^{-1}\left[1+\frac{i}{2X}\left(\frac{1}{m-1}-\frac{m-1}{m}\right)\right]X^{-1}$$

$$\times \exp[2i(m-1)X] - \tfrac{1}{2}(m-1)\sum_{j=1}^{\infty}\left[j-\left(\frac{m-1}{2}\right)\right]^{-1}\left(\frac{m-1}{m+1}\right)^{2j}$$

$$\left.\times \exp\left[2i\,(m-1+2jm)X\right]\right\} - 0.7153537X^{-\frac{4}{3}}$$

$$- 0.3320643\,\mathrm{Im}\left[e^{\frac{i\pi}{3}}(m^2-1)^{-\frac{3}{2}}(m^2+1)(2m^4-6m^2+3)\right]X^{-\frac{5}{3}}$$

$$+ o(X^{-2}) + \text{ripple} \qquad . \qquad \text{(A-22)}$$

Q_{abs} is given by

$$Q_{abs} = \langle Q_{abs}\rangle_F + \langle Q_{abs}\rangle_{a_\bullet e_\bullet} + \langle Q_{abs}\rangle_{b_\bullet e_\bullet} \qquad \text{(A-23)}$$

where

$$\langle Q_{abs}\rangle_F = \sum_{\lambda=1}^{2}\int_0^{\frac{\pi}{2}}\phi\left(r_{j\lambda}\right)\sin\theta\cos\theta\,d\theta \qquad \text{(A-24)}$$

$$\langle Q_{abs}\rangle_{a_\bullet e_\bullet} = 2^{-\frac{1}{3}}X^{-\frac{2}{3}}\sum_{\lambda=1}^{2}\int_0^{x_a}\phi\left(r_{j\lambda}^{+}\right)dx \qquad \text{(A-25)}$$

and

$$\langle Q_{abs}\rangle_{b_\bullet e_\bullet} = 2^{-\frac{1}{3}}X^{-\frac{2}{3}}\sum_{\lambda=1}^{2}\int_0^{x_b}\left[\phi\left(r_{j\lambda}^{-}\right)-\phi\left(\bar{r}_{j\lambda}^{-}\right)\right]dx \qquad . \qquad \text{(A-26)}$$

In Eqs. A-24 through A-26,

$$\phi(r_{j\lambda}) = (1 - e^{-b})(1 - r_{2\lambda}) / (1 - r_{1\lambda}e^{-b}) \qquad \text{(A-27)}$$

where

$$r_{j\lambda} = |R_{j\lambda}|^2, \quad j, \lambda = 1, 2; \quad R_{j\lambda} = (-1)^j (z_j - ue_\lambda) / (z + ue_\lambda) \qquad \text{(A-28)}$$

$$z = \cos\theta, \quad u = m\cos\theta', \quad \sin\theta = m\sin\theta', \qquad \text{(A-29)}$$

$$e_1 = 1, \quad e_2 = m^{-2}, \quad z_1 = z, \quad z_2 = \begin{cases} z \text{ for Eq. A-24} \\ z^* \text{ for Eqs. A-25 and A-26} \end{cases} \qquad \text{(A-30)}$$

and finally,

$$b = 4X\,\mathrm{Im}(m\cos\theta' + \theta'\sin\theta) \qquad \text{(A-31)}$$

Equations for the Bohren and Nevitt Approximation[10]

The Bohren and Nevitt approximation for Q_{abs} is computed as

$$Q_{abs} = \frac{4n^3}{(n+1)^2 - (n-1)^2\exp(-\tau)} \left\{ \frac{1}{n^2} - \frac{2}{\tau^2} \left[\exp\left(\frac{-\tau\sqrt{n^2-1}}{n} \right) \right.\right.$$

$$\left.\left. \times \left(\frac{1 + \tau\sqrt{n^2-1}}{n} \right) - \exp(-\tau)\,(1+\tau) \right] \right\} \qquad \text{(A-32)}$$

where

$$\tau = 4kX \qquad \text{(A-33)}$$

Equations for the Levine Approximation[11]

The Levine approximation for Q_{abs} is computed as

$$Q_{abs} = 2(1 - A)[H(4kX) + H(B) - H(4kX + B)] \qquad \text{(A-34)}$$

where the function H(u) is given by

$$H(u) = \frac{1}{2} + \frac{e^{-u}}{u} + \frac{e^{-u} - 1}{u^2} \qquad \text{(A-35)}$$

and

$$B = \frac{2n\left[1 + \frac{2}{(n^2 + k^2)}\right]}{1 - A} \qquad \text{(A-36)}$$

The value for A in Eqs. A-34 and A-36 is determined using an iterative scheme given by

$$A = R + (A - 1)\exp\left[\frac{-2n\left(1 + \frac{2}{n^2 + k^2}\right)}{1 - A}\right] \qquad \text{(A-37)}$$

where the iteration is begun with $A^{(0)} = R$ and

$$R = \left[\frac{(n - 1)^2 + k^2}{(n + 1)^2 + k^2}\right] \qquad \text{(A-38)}$$

*U.S. GOVERNMENT PRINTING OFFICE